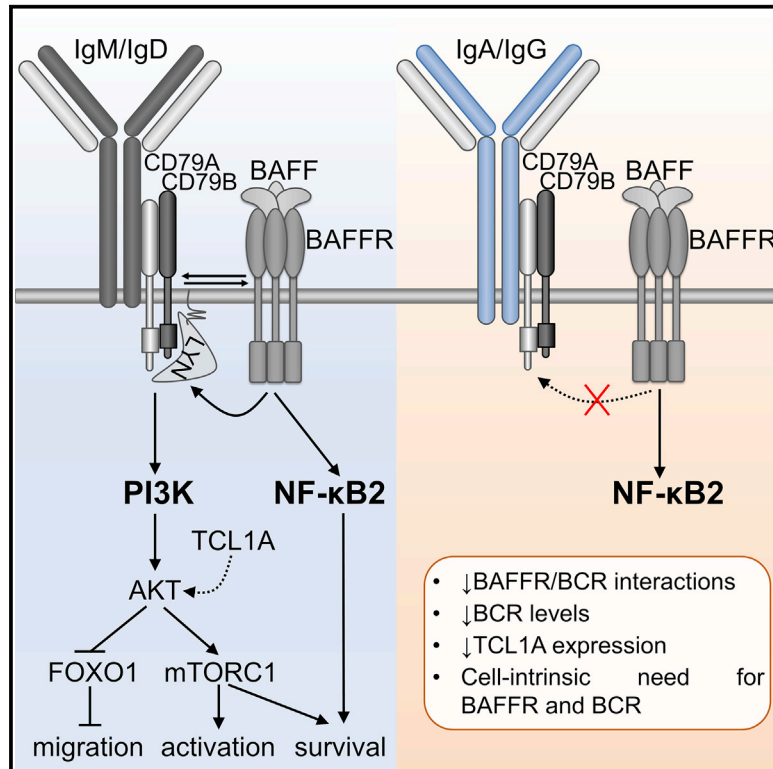


## BAFFR activates PI3K/AKT signaling in human naive but not in switched memory B cells through direct interactions with B cell antigen receptors

### Graphical abstract



### Authors

Eirini Sevdali, Violeta Block, Marie Lataretu, ..., Martin Hölzer, Pascal Schneider, Hermann Eibel

### Correspondence

hermann.eibel@uniklinik-freiburg.de

### In brief

Sevdali et al. show that human mature B cells express BAFFR. Since BAFFR interacts stronger with BCRs of naive than of memory B cells, BAFF regulates pro-survival responses only in naive B cells, while both subsets have a BAFF-independent cell-intrinsic requirement for BAFFR expression.

### Highlights

- BAFFR interacts strongly with BCRs of naive but not of memory B cells
- BAFFR activates PI3K signaling via LYN in naive but not in memory B cells
- BAFF regulates in naive B cells >300 genes for growth, proliferation, and migration
- Inactivation of *BAFFR* or of *CD79A/B* induces apoptosis in naive and memory B cells



## Article

# BAFFR activates PI3K/AKT signaling in human naive but not in switched memory B cells through direct interactions with B cell antigen receptors

Eirini Sevdali,<sup>1,2,3</sup> Violeta Block,<sup>1,2,3</sup> Marie Lataretu,<sup>4</sup> Huiying Li,<sup>1,2,3</sup> Cristian R. Smulski,<sup>5</sup> Jana-Susann Briem,<sup>1,2,3</sup> Yannic Heitz,<sup>1,2,3</sup> Beate Fischer,<sup>1,2,3</sup> Neftali-Jose Ramirez,<sup>2,3,6</sup> Bodo Grimbacher,<sup>2,3,6</sup> Hans-Martin Jäck,<sup>7</sup> Reinhard E. Voll,<sup>1,2,3</sup> Martin Hölzer,<sup>8</sup> Pascal Schneider,<sup>9</sup> and Hermann Eibel<sup>1,2,3,10,\*</sup>

<sup>1</sup>Department of Rheumatology and Clinical Immunology, Medical Center – University of Freiburg, Hugstetterstr. 55, 79106 Freiburg, Germany

<sup>2</sup>Faculty of Medicine, University of Freiburg, Breisacherstr. 153, 79110 Freiburg, Germany

<sup>3</sup>Center for Chronic Immunodeficiency, Medical Center – University of Freiburg, Breisacherstr. 115, 79106 Freiburg, Germany

<sup>4</sup>RNA Bioinformatics and High-Throughput Analysis, Faculty of Mathematics and Computer Science, University of Jena, Leutragraben 1, 07743 Jena, Germany

<sup>5</sup>Medical Physics Department, Centro Atómico Bariloche, Comisión Nacional de Energía Atómica (CNEA), Consejo Nacional de Investigaciones Científicas y Técnicas (CONICET), Avenida E-Bustillo 9500, R8402AGP Río Negro, San Carlos de Bariloche, Argentina

<sup>6</sup>Institute for Immunodeficiency, Medical Center – University of Freiburg, Breisacherstr. 115, 79106 Freiburg, Germany

<sup>7</sup>Department of Medicine, Division of Immunology, University of Erlangen, Glückstraße 6, 91054 Erlangen, Germany

<sup>8</sup>Methodology and Research Infrastructure, MF1 Bioinformatics, Robert Koch Institute, Nordufer 20, 13353 Berlin, Germany

<sup>9</sup>Department of Biochemistry, University of Lausanne, Ch. des Boveresses 155, 1066 Epalinges, Switzerland

<sup>10</sup>Lead contact

\*Correspondence: [hermann.eibel@uniklinik-freiburg.de](mailto:hermann.eibel@uniklinik-freiburg.de)

<https://doi.org/10.1016/j.celrep.2022.111019>

## SUMMARY

Binding of BAFF to BAFFR activates in mature B cells PI3K/AKT signaling regulating protein synthesis, metabolic fitness, and survival. In humans, naive and memory B cells express the same levels of BAFFR, but only memory B cells seem to survive without BAFF. Here, we show that BAFF activates PI3K/AKT only in naive B cells and changes the expression of genes regulating migration, proliferation, growth, and survival. BAFF-induced PI3K/AKT activation requires direct interactions between BAFFR and the B cell antigen receptor (BCR) components CD79A and CD79B and is enhanced by the AKT coactivator TCL1A. Compared to memory B cells, naive B cells express more surface BCRs, which interact better with BAFFR than IgG or IgA, thus allowing stronger responses to BAFF. As ablation of BAFFR in naive and memory B cells causes cell death independent of BAFF-induced signaling, BAFFR seems to act also as an intrinsic factor for B cell survival.

## INTRODUCTION

Long-lived, class-switched memory B cells (MBCs) form an important pillar of the humoral immune response and can persist in humans for decades (Yu et al., 2008). However, the mechanisms regulating their longevity are not well understood. BAFF receptor (BAFFR) and its ligand BAFF are essential regulators of B cell survival (Mackay and Schneider, 2009; Schweighoffer and Tybulewicz, 2018). BAFFR expression starts in immunoglobulin M-positive (IgM<sup>+</sup>) immature B cells (Smith and Cancro, 2003) and increases to equally high levels in mature follicular, marginal zone (MZ) and switched MBCs (Darce et al., 2007), except for plasma cells and centroblasts, which do not express BAFFR (Smulski et al., 2017). BAFF is mainly produced by monocytes, fibroblastic reticular cells, and activated T cells (Cremasco et al., 2014; Moore et al., 1999; Nardelli et al., 2001) and binds apart from BAFFR to two other receptors, TACI and BCMA (Gross et al., 2000).

*Baff*<sup>-/-</sup> and *Baffr*<sup>-/-</sup> mice (Sasaki et al., 2004; Schiemann et al., 2001) or BAFFR deficiency in humans (Warnatz et al., 2009) are characterized by impaired B cell survival from the transitional B cell stage on, resulting in B cell lymphopenia, low IgG and IgM titers, and defective humoral immune responses. As BAFFR deficiency does not prevent the generation of mucosal IgA-secreting plasma cells (Sasaki et al., 2004; Warnatz et al., 2009), these cells can develop without BAFFR signaling. BAFFR variants altering receptor oligomerization and signaling correlate with primary immunodeficiency, lymphomas, and autoimmunity (Hildebrand et al., 2010; Losi et al., 2005; Ntellas et al., 2020; Pieper et al., 2014), whereas high BAFF levels are linked to autoimmunity (Mackay et al., 1999; Steri et al., 2017). Since BAFF supports the survival of autoreactive B cells (Cancro, 2009; Thien et al., 2004), BAFF-neutralizing antibodies (belimumab, approved) and soluble TACI decoy receptors (atacicept) have been tried and are used in humans. As they eliminate most circulating naive and MZ B cells but spare MBCs, at least



a fraction of human MBCs can survive for >1 year without BAFF (Jacobi et al., 2010; Stohl et al., 2012; Tak et al., 2008).

BAFF binding to BAFFR activates the nuclear factor  $\kappa$ B (NF- $\kappa$ B) inducing kinase (NIK), leading to the phosphorylation of the NF- $\kappa$ B2 precursor p100 and its proteolytic cleavage into active p52 (Claudio et al., 2002). Thus, NIK and NF- $\kappa$ B2 deficiency also block, like BAFFR deficiency, B cell development from the transitional B cell stage on (Chen et al., 2013; Willmann et al., 2014). Moreover, BAFFR activates protein kinase C (PKC) (Mecklenbrauker et al., 2004), extracellular signal-regulated kinase (ERK) (Jacque et al., 2015; Otipoby et al., 2008), and the phosphoinositide 3-kinase (PI3K) pathway (Patke et al., 2006). BAFF-induced PI3K activation requires components of the B cell receptor (BCR) signalosome such as CD79A, SYK, and CD19 (Hobeika et al., 2015; Schweighoffer et al., 2013). PI3K generates phosphatidylinositol-3,4,5-trisphosphate (PIP3) serving as a plasma membrane anchor for the serine/threonine kinase AKT, which controls protein synthesis, metabolic fitness, proliferation, and survival (Patke et al., 2006; Woodland et al., 2008).

Most BAFF-induced signaling responses were studied in mice, and because human naive B cells require BAFF/BAFFR to survive (Stohl et al., 2012; Warnatz et al., 2009), it is assumed that BAFF activates human B cells in a way similar to that of mouse B cells. However, as human MBCs survive without BAFF for months if not years (Furie et al., 2018), we investigated whether BAFFR signaling would differ between human naive and MBCs.

Here, we show that in naive B cells, BAFF rapidly induced PI3K signaling and regulated the expression of hundreds of genes involved in cell survival, activation, and migration, while MBCs remained almost unresponsive. The direct interactions between BAFFR and the BCR signaling subunits CD79A/CD79B appeared to be one of the decisive factors in BAFF-induced PI3K signaling. Since BAFFR-BCR interactions were weaker for IgG and IgA BCRs than for IgM, and because MBCs expressed less surface BCRs than naive B cells, and, in addition, much lower levels of the AKT co-activator T-cell leukemia/lymphoma protein 1A (TCL1A), BAFF activated PI3K in naive B cells but not in MBCs. Although human MBCs survive *in vivo* without BAFF/BAFFR signaling, they tolerated neither the genetic inactivation of BAFFR nor of CD79A or CD79B. Therefore, BAFFR seems to be, like the BCR, an essential structural component required for the survival of mature B cells in humans.

## RESULTS

### BAFF promotes the survival of naive but not switched MBCs

BAFF-independent survival of MBCs was analyzed by comparing circulating B cell subsets of patients with systemic lupus erythematosus (SLE) treated for >6 months with belimumab to those of controls (Figures 1A and S1A–S1C). BAFFR expression was comparable in all of the subsets and samples (Figure 1A), but while approximately 4%–8% of lymphocytes of healthy donors were IgD<sup>+</sup> CD27<sup>-</sup> naive B cells, belimumab-treated SLE patients had only 0.2%–2% circulating naive B cells. On the contrary, the percentages of IgD<sup>-</sup> IgM<sup>+</sup> CD27<sup>+</sup>, IgG<sup>+</sup>, and IgA<sup>+</sup> MBCs did not

differ significantly between patients and controls (Figure S1C), suggesting that the neutralization of BAFF affects mainly naive B cells but not MBCs.

To investigate these BAFF-related differences between naive and MBCs in more detail, we performed a series of *in vitro* activation and survival assays. Treatment with BAFF increased the size and supported the survival of naive B cells, but not of MBCs (Figures 1B–1D and S1D). The addition of belimumab or of human TACI-Fc (hTACI-Fc) (Vigolo et al., 2018) blocked BAFF binding to all B cells and prevented BAFF-induced survival of naive B cells, confirming that B cells did not produce endogenous BAFF, which would have masked the activity of recombinant BAFF (Figures S1E and S1F). In addition, BAFF induced the expression of the activation markers CD69 and CD83 in >60% of naive B cells, while only 40% of MBCs upregulated CD83 (Figures 1E and 1F). As >90% of MBCs highly expressed both markers in response to CD40L (Figures S1G and S1H), a status of general unresponsiveness was ruled out.

Since CD69 inhibits sphingosine-1-phosphate receptor (S1PR1) activity, and thus S1P-mediated migration of human B cells (Sic et al., 2014), we therefore tested whether BAFF-induced CD69 expression would prevent S1P1-dependent migration. Both CD69<sup>+</sup> naive B cells and MBCs did not migrate in response to S1P, but because BAFF increased the percentage of CD69<sup>+</sup> naive B cells approximately 2-fold, it reduced the fraction of cells capable of migrating toward S1P (Figure S1I).

Thus, the persistence of MBCs in the belimumab-treated SLE patients and the weak *in vitro* activation of healthy donor MBCs by BAFF strongly supported our initial hypothesis that the response of MBCs to BAFF differs from naive B cells, which need BAFF to survive.

### BAFF-induced changes in gene expression

As the BAFF-induced changes in naive cells could reflect transcriptional changes, we compared by RNA sequencing (RNA-seq) the transcriptomes of naive B cells and MBCs from 4 healthy donors after 6 h of activation with BAFF.

Principal-component analysis of the top 500 varying genes showed a clear clustering of BAFF-treated versus untreated naive B cells, whereas MBCs clustered mainly according to the donors and not treatment (Figure 2A). In naive B cells, BAFF changed the expression of 331 protein coding genes at least 2-fold (Figures 2B and S2A–S2C). Applying STRING as a tool for functional and direct interactions between proteins, several groups of differentially expressed genes were identified (Figures S2D and S2E) regulating transcription (*POLR1C*, *SNAPC4*), pre-rRNA processing, nucleolar assembly, and ribosome biogenesis (*NOLC1*, *DKC1*, *EBNA1BP2*, *TSR1*, *WDR12*, *NIP7*, *MRTO4*, *PNO1*). This suggests that protein synthesis is one of the early targets of BAFFR activation. BAFF also upregulated transcripts encoding cell-cycle regulators (*CDK4*, *CCND2*), transcription factors (*MYC*, *STAT5A*, *IRF4*), anti-apoptotic proteins (*BCL2L1*, *BCL2A1*), chemokines and interleukins (*CCL4*, *IL1B*, *IL10*, *IL6*). In addition, BAFF downregulated genes controlling lymphocyte migration (*S1PR1*, *SELL*, *PECAM1*, *KLF2*), encoding inhibitory receptors (*FCGR2B*, *LPAR5*), phosphatases (*INPP5D*), or guanine-nucleotide binding proteins (*GNB5*;

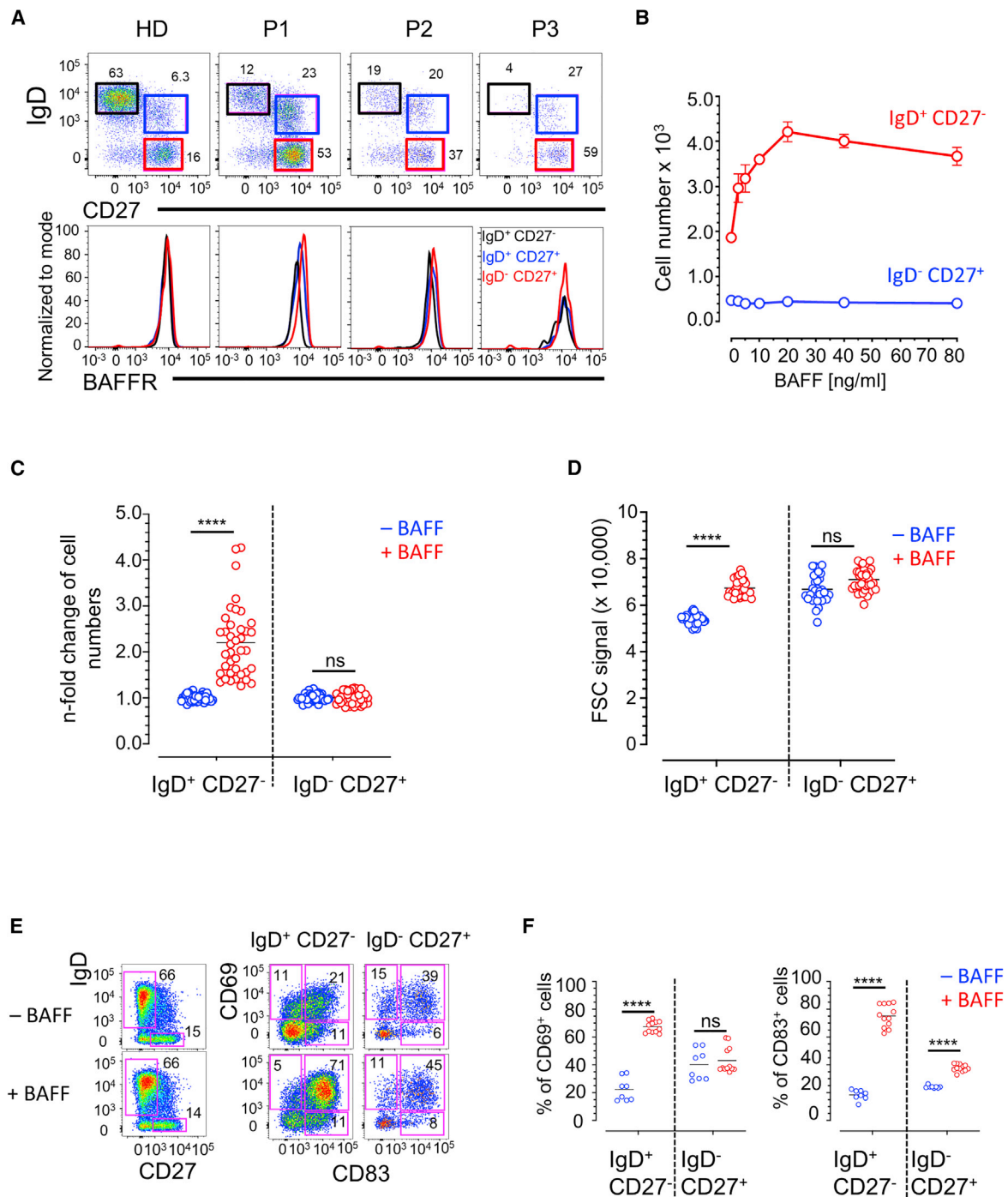


**Figure 1. BAFF promotes the survival of naive but not switched memory B cells (MBCs)**

(A) Flow cytometric analysis of naive (IgD<sup>+</sup> CD27<sup>-</sup>), MZ (IgD<sup>+</sup> CD27<sup>+</sup>), and memory (IgD<sup>-</sup> CD27<sup>+</sup>) B cells of a healthy donor (HD) and SLE patients treated with belimumab for >6 months (P1–P3). Histogram overlays display BAFFR expression by the different subsets. See also Figures S1A–S1B.

(B) Cell numbers of B cell subsets treated with BAFF in a dose-dependent manner for 3 days were analyzed by flow cytometry and timed acquisition. Means ± SDs of 1 out of 3 independent experiments.

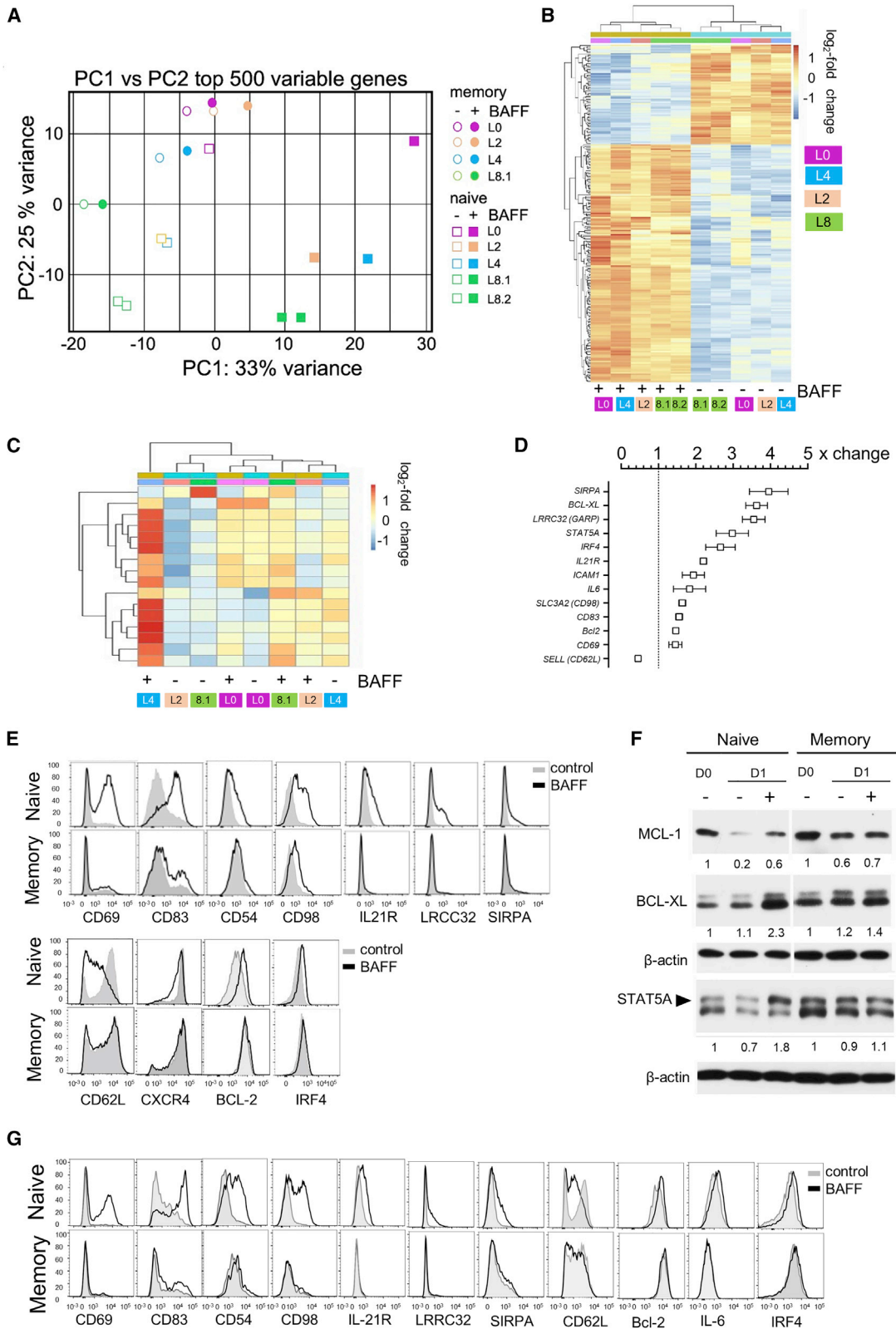
(C) Similar to (B), showing n-fold changes of cell numbers ± BAFF (20 ng/mL) calculated as (cell number + BAFF/cell number – BAFF).

(D) Similar to (C), showing changes in forward scatter (FSC). (C and D) >6 independent experiments (3 technical replicates/experiment, 5 HDs).

(E and F) Flow cytometric analysis of CD69 and CD83 expression upon overnight treatment of B cells ± BAFF (E). (F) Data of 6 independent experiments (2 technical replicates/experiment, 2 HDs).

(C, D, and F) \*\*\*\*p < 0.0001; ns, not significant (2-way ANOVA with Tukey multiple comparisons test). Horizontal lines show the mean.

See also Figure S1.



(legend on next page)

Figures 2D, S2D, and S2E). Thus, activation of BAFFR thoroughly changed within 6 h the physiological status of naive B cells.

In contrast to naive B cells, BAFF binding to MBCs changed the expression of only a dozen genes (Figures 2C and S2C), approximately 50% (e.g., CD83) of which were also detected in naive B cells.

Analysis of the protein expression of some of these genes showed that overnight treatment with BAFF significantly increased in naive B cells the levels of CD69, CD83, CD54, CD98, interleukin-21R (IL-21R), LRCC32, SIRP $\alpha/\beta$ , signal transducer and activator of transcription 5A (STAT5A), and less but reproducibly of CCL3, CCL4, IL-6, IL-10, IL-1 $\beta$ , interferon regulatory factor-4 (IRF-4), while it decreased the expression of CD62L and CXCR4. In naive B cells, BAFF upregulated the expression of the anti-apoptotic factors BCL-2 and BCL-XL to approximately the same levels as were found in resting MBCs, while it prevented the degradation of MCL-1 *in vitro*. In MBCs, none of these genes changed their expression in response to BAFF, with the exception of CD83 and of CD98, which were slightly increased (Figures 2E and 2F and S2F). Since these expression patterns did not change after 2 days of BAFF treatment, it is unlikely that MBCs respond slower than naive B cells (Figure 2G).

BAFF upregulated STAT5A and IL-21R expression, two essential signaling components of IL-21-dependent B cell proliferation (Habib et al., 2002). We therefore tested whether BAFF would synergize with IL-21 to activate cell division. BAFF-induced expression of IL-21R in naive B cells allowed their proliferation in combination with IL-21, although not as strongly as with CD40L and IL-21 (Figure S2G). MBCs upregulated IL-21R only in response to CD40L, which together with IL-21 led to their vigorous proliferation. Thus, BAFF primed naive but not MBCs for IL-21-induced proliferation. Therefore, the extremely weak response of MBCs to BAFF seems to be a specific feature of these cells, even though they express the two BAFF receptors BAFFR and TACI.

### BAFF differently activates PI3K signaling in naive and MBCs

To better understand the differences between naive and MBCs in responding to BAFF, we compared the activation of NF- $\kappa$ B2 and PI3K pathways. Since BAFF induced the processing of NF- $\kappa$ B2 p100 into active p52 in both subsets (Figure 3A), we

blocked NIK activity (Figure S3A) to determine whether NF- $\kappa$ B2 would regulate BAFF-induced survival. While NIK inhibition decreased BAFF-dependent survival of naive B cells by approximately 50%, it had no effect on MBCs (Figure 3B). Thus, the survival of MBCs does not depend on BAFF-induced NIK/NF- $\kappa$ B2 activity.

BAFF binding to BAFFR also activates PI3K signaling using components of the BCR pathway (Hobeika et al., 2015; Jellusova et al., 2013; Schweighoffer et al., 2013). In naive B cells, BAFF rapidly induced the phosphorylation of CD79A (Y188). This was followed by the phosphorylation of other substrates downstream of PI3K, including AKT (S473), the ribosomal protein S6 (S240/244), and the translational repressor 4EBP1 (S65) (Figures 3C and S3B–S3D). Unlike naive B cells, MBCs did not respond to BAFF, but the higher basal pS6 levels could be an indication for higher protein synthesis (Figures 3C, S3B, and S3C). In naive B cells, anti-IgM treatment induced a stronger phosphorylation of CD79A, SYK (Y525/526), and S6 than BAFF, but not of CD19 (Y531) (Figure 3D). As CD40L induced the phosphorylation of S6 and 4EBP1 in MBCs as strongly as in naive B cells (Figures S3C and S3D), activation of the PI3K pathway was not generally impaired in MBCs.

BAFF rapidly induced the phosphorylation of CD79A and CD19 in naive B cells (Figures 3C and 3D). Therefore, we tested whether the BCR-associated SRC kinase LYN would initiate PI3K activation downstream of BAFFR by analyzing its transition from the autoinhibitory (pY508) to active (pY397) state (Gaul et al., 2000; Rolli et al., 2002). Using BAFFR-expressing DG-75 Burkitt's lymphoma cells as a model, we found that BAFF induced the dephosphorylation of LYN (Y508) within 2 min, followed by the phosphorylation of Y397 (Figure 3E). This was a critical step in initiating the PI3K pathway as inactivation of LYN by CRISPR-Cas9 mutagenesis or inhibition of the kinase activity by the dual BCR-ABL/LYN inhibitor bafetinib (Kimura et al., 2005) almost completely abolished AKT phosphorylation (Figure 3F). Since the effect of bafetinib in anti-IgM-induced AKT phosphorylation was weaker, BCR crosslinking activates other SRC kinases (Figure 3F).

Although the inhibition of LYN blocked BAFF-induced AKT and S6 phosphorylation, it did not completely inhibit CD19 phosphorylation (Figure 3G). Thus, BAFF may also activate additional SRC kinases in primary B cells. As SYK amplifies the initial

### Figure 2. BAFF-induced changes in gene expression

(A) Principal-component analysis of BAFF-activated B cells. B cells of 4 HDs (L0, L2, L4, L8) were separated into naive (with 2 replicates of donor L8: L8.1, L8.2) and MBCs (L0, L2, L4, L8.1), activated for 6 h with BAFF (20 ng/mL) and analyzed by RNA-seq. The 4 donors L0–L8 are color coded, empty symbols represent controls, and filled symbols represent BAFF-activated samples. Changes in gene expression between naive (squares) and MBCs (circles) are displayed as principal-component analysis of normalized RNA-seq reads of the 500 most varying genes. Enrichment of naive and MBCs was confirmed by analyzing subset-specific transcripts (see Figure S2A).

(B) Heatmap displaying log<sub>2</sub>-fold changes of normalized RNA-seq counts in naive B cells. Full clustering was calculated according to stimulation ( $\pm$ BAFF, columns) and genes (rows); color coding as in (A).

(C) Same as in (B), showing log<sub>2</sub>-fold changes of normalized RNA-seq counts in MBCs. Clustering and coding as in (A) and (B).

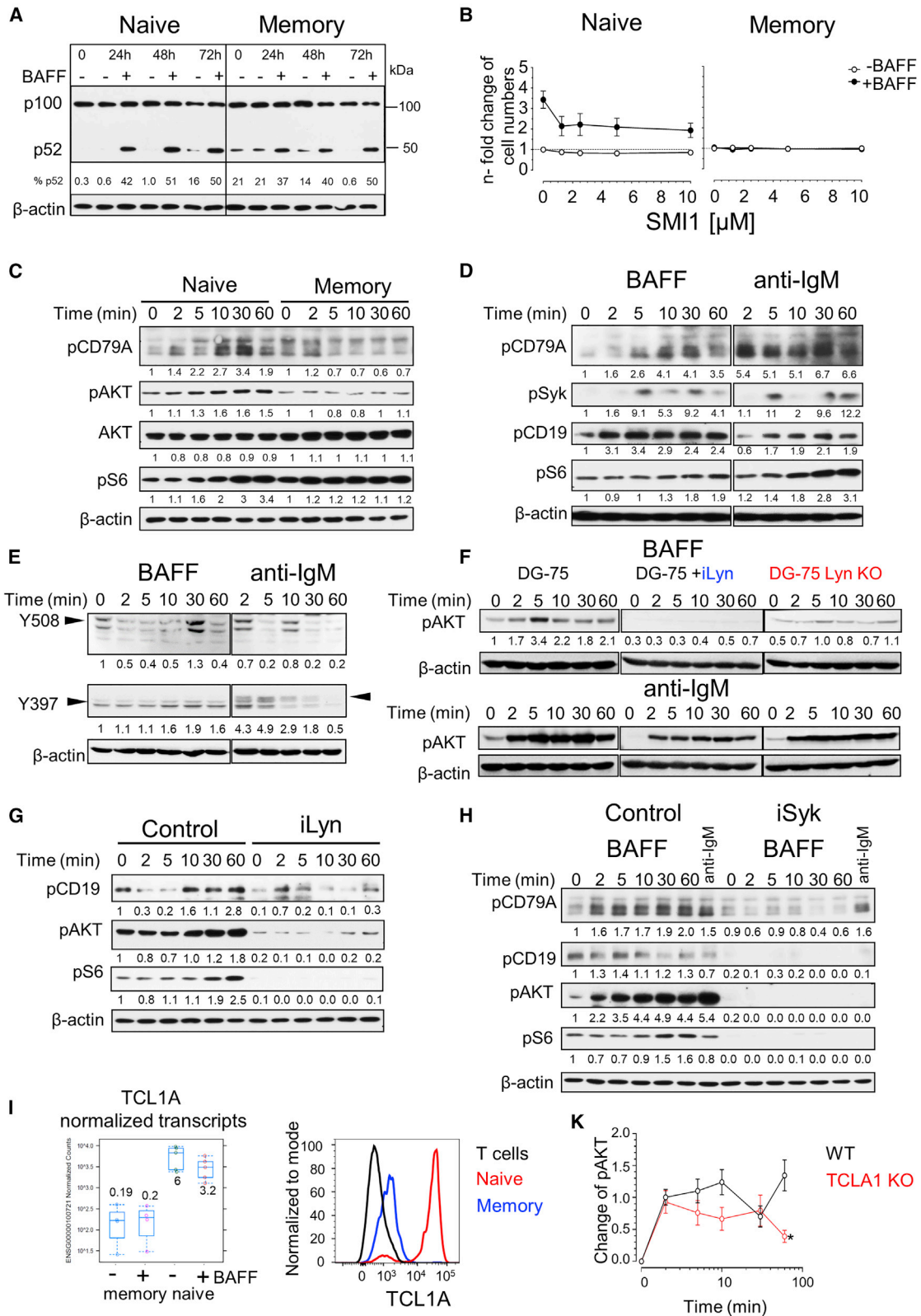
(D) BAFF-induced relative changes (means  $\pm$  SDs) in transcript levels of selected genes expressed by naive B cells analyzed at protein level as shown in (E)–(G).

(E) Histogram overlays of proteins analyzed by flow cytometry in naive and MBCs after overnight treatment with BAFF (black line) compared to controls (gray line). (F) Western blot analysis of MCL-1, BCL-XL, and STAT5 in naive and MBCs treated with BAFF overnight. N-fold change was calculated as signals normalized to actin and further normalized to untreated samples from day 0 for each subset.

(G) Same as in (E), 2 days after BAFF treatment.

(E–G) Data are representative of  $\geq 2$  independent experiments ( $\geq 2$  technical replicates, 2 HDs).

See also Figure S2.



(legend on next page)

activation signals of LYN (Klasener et al., 2014; Rolli et al., 2002), we tested whether blockade of SYK would prevent BAFF-induced phosphorylation of CD79A, CD19, AKT, and S6 in naive B cells. As shown in Figure 3H, the inhibition of SYK completely blocked the phosphorylation of these proteins. Thus, the BAFF-dependent activation of the PI3K signaling cascade in naive B cells made use of BCR signaling components.

The small protein TCL1A can assemble into homodimers that serve as docking sites for AKT, augmenting its activation (Laine et al., 2000; Pekarsky et al., 2000). Since the transcripts and protein levels of TCL1A were 25–30 times higher in naive B cells than in MBCs (Figure 3I), this difference could explain why BAFF can activate PI3K/AKT signaling in naive B cells but not in MBCs. Therefore, we tested whether the inactivation of *TCL1A* by CRISPR-Cas9 mutagenesis (Figure S3E) would change BAFF-induced AKT S473 phosphorylation in DG-75 cells. As shown in Figure 3K, AKT phosphorylation was reduced but not abolished in *TCL1A* KO DG-75 cells.

In naive B cells, inactivation of *TCL1A* impaired BAFF-induced upregulation of CD69 (Figure S3F). Interestingly, the *TCL1A*<sup>−</sup> cells of mock electroporated control samples also failed to upregulate CD69 after stimulation with BAFF. Since the BAFF-induced increase in CD69 expression depends on PI3K activity (Figure S3G), very low levels of *TCL1A* in MBCs could explain why BAFF did not induce phosphorylation of AKT and its downstream substrate proteins in MBCs. However, inactivation of *TCL1A* did not impair BAFF-dependent and independent survival of naive B cells *in vitro* (Figure S3H).

As BAFF induced within 6 h the expression of BCL-2, BCL-XL, and MCL-1 (Figures 2D–2F and S3I), we tested whether they are regulated by PI3K and by NIK using the PI3K $\delta$ - and NIK-specific inhibitors nemoralisib and SMI1, respectively. The inhibition of PI3K $\delta$  reduced the BAFF-dependent increase in BCL-2, BCL-XL, and MCL1 levels by approximately 30%–50% in naive B cells. Inhibition of NIK mainly decreased BAFF-induced BCL-2 expression, whereas MBCs did not change the levels of any

of these BCL-2 family members in response to BAFF (Figures S3K and S3L). Different from BAFF, the inhibition of NIK or PI3K $\delta$  had little effect on the CD40L-dependent induction of MCL1 or BCL-XL (Figure S3L). Consequently, BAFF activates the BCR-associated kinases LYN and SYK as well as PI3K signaling and controls the expression of critical anti-apoptotic proteins in naive B cells but not in MBCs.

### BAFF-induced PI3K signaling regulates phosphatase and tensin homolog (PTEN) and forkhead box O1 (FOXO1) in naive B cells

The weak activation of the PI3K pathway in MBCs by BAFF could also result from the high expression levels of the PI3K antagonist PTEN (Maehama and Dixon, 1998; Stambolic et al., 1998). Comparing PTEN expression in naive and MBCs, we detected similar levels in both subsets, which increased approximately 3-fold in response to BAFF in naive B cells (Figures 4A and 4B).

PTEN regulates the activation of the transcriptional factor FOXO1 (Song et al., 2012), which controls B cell proliferation and apoptosis (Yusuf et al., 2004). Resting naive B cells expressed slightly higher levels of FOXO1 than MBCs, which were maintained by BAFF *in vitro* (Figure 4A). However, the increased PTEN and FOXO1 levels in naive B cells following treatment with BAFF were regulated by the PI3K pathway, as shown by inhibiting SYK, PI3K $\delta$ , and PDK1 (Figures 4D and 4E). This suggests that BAFF can also limit prolonged naive B cell activation by increasing PTEN and FOXO1 expression.

BAFF-induced activation of AKT in naive B cells also resulted in the rapid transient phosphorylation of FOXO1 (Figure 4C), which inactivates the transcription factor (Matsuzaki et al., 2003). Since FOXO1 controls the expression of CXCR4 and CD62L either directly or indirectly by regulating other transcriptional factors such as the KLF2 (Chen et al., 2010; Dengler et al., 2008; Dominguez-Sola et al., 2015; Fabre et al., 2008; Lou et al., 2012; Sander et al., 2015), we tested whether BAFF-induced downregulation of CD62L and CXCR4 would depend

### Figure 3. BAFF differently activates naive and MBCs

- (A) Western blot analysis of NF- $\kappa$ B2 processing in naive and MBCs treated with BAFF (20 ng/mL) for 24–72 h. The percentage of processed NF- $\kappa$ B2 was calculated as [(signal of p52)/(signal of p52 + signal of p100)]  $\times$  100.
- (B) N-fold change of cell numbers of naive and MBCs treated  $\pm$  BAFF in the presence of the NIK inhibitor SMI1 (1.25–10  $\mu$ M) or DMSO for 3 days, calculated as (cell number  $\pm$  inhibitor  $\pm$  BAFF/cell number in DMSO-BAFF). Means  $\pm$  SEMs of 2 independent experiments (3 technical replicates/experiment, 2 HDs).
- (C) Western blot analysis of phosphorylated CD79A (Y188), AKT (S473), S6 (S240/244), and total AKT in naive and MBCs activated with BAFF for 2–60 min. Data are representative of  $\geq$  3 HDs.
- (D) Western blot analysis of pCD79A, pSYK (Y525/526), pCD19 (Y531), and pS6 in naive B cells treated with BAFF or F(ab')<sub>2</sub> anti-IgM (2  $\mu$ g/mL). Data are representative of 2 HDs.
- (E) Western blot analysis of pLYN (Y508, Y397) in DG-75 cells treated with BAFF (100 ng/mL) or F(ab')<sub>2</sub> anti-IgM (2  $\mu$ g/mL). Data are representative of 2 independent experiments.
- (C–E) N-fold changes in protein expression were calculated as signals normalized to actin and further normalized to untreated samples.
- (F) Western blot analysis of pAKT in LYN KO or WT DG-75 cells treated with BAFF or F(ab')<sub>2</sub> anti-IgM in the presence of the LYN inhibitor bafetinib (10  $\mu$ M) or DMSO. Data are representative of 3 independent experiments. N-fold changes of pAKT signals were relative to untreated DG-75 cells (t = 0).
- (G) Western blot analysis of pCD19, pAKT, and pS6 in naive B cells activated with BAFF in the presence of bafetinib (10  $\mu$ M) or DMSO (control).
- (H) Similar to (G), showing pCD79A, pCD19, pAKT, and pS6 in naive B cells treated with BAFF (2–60 min) or F(ab')<sub>2</sub> anti-IgM (5 min) in the presence of the SYK inhibitor R406 (2.5  $\mu$ M) or DMSO.
- (G and H) N-fold changes in phosphorylated proteins were calculated as signals normalized to actin and further normalized to the control sample at t = 0.
- (I) *TCL1A* transcript (left) and protein (right) levels assessed by RNA-seq and intracellular flow cytometry in naive and MBCs of a HD; T cells: control.
- (K) Changes in pAKT values analyzed by western blot in wild-type (WT) and *TCL1A* KO DG-75 cells treated with BAFF (2–60 min) were calculated as [(signal t<sub>x</sub> – signal t<sub>0</sub>)/signal t<sub>0</sub>]. pAKT signals were previously normalized to actin. Plot shows the means  $\pm$  SEMs of  $\geq$  5 independent experiments. \*p < 0.05 (Mann-Whitney test).

See also Figure S3.

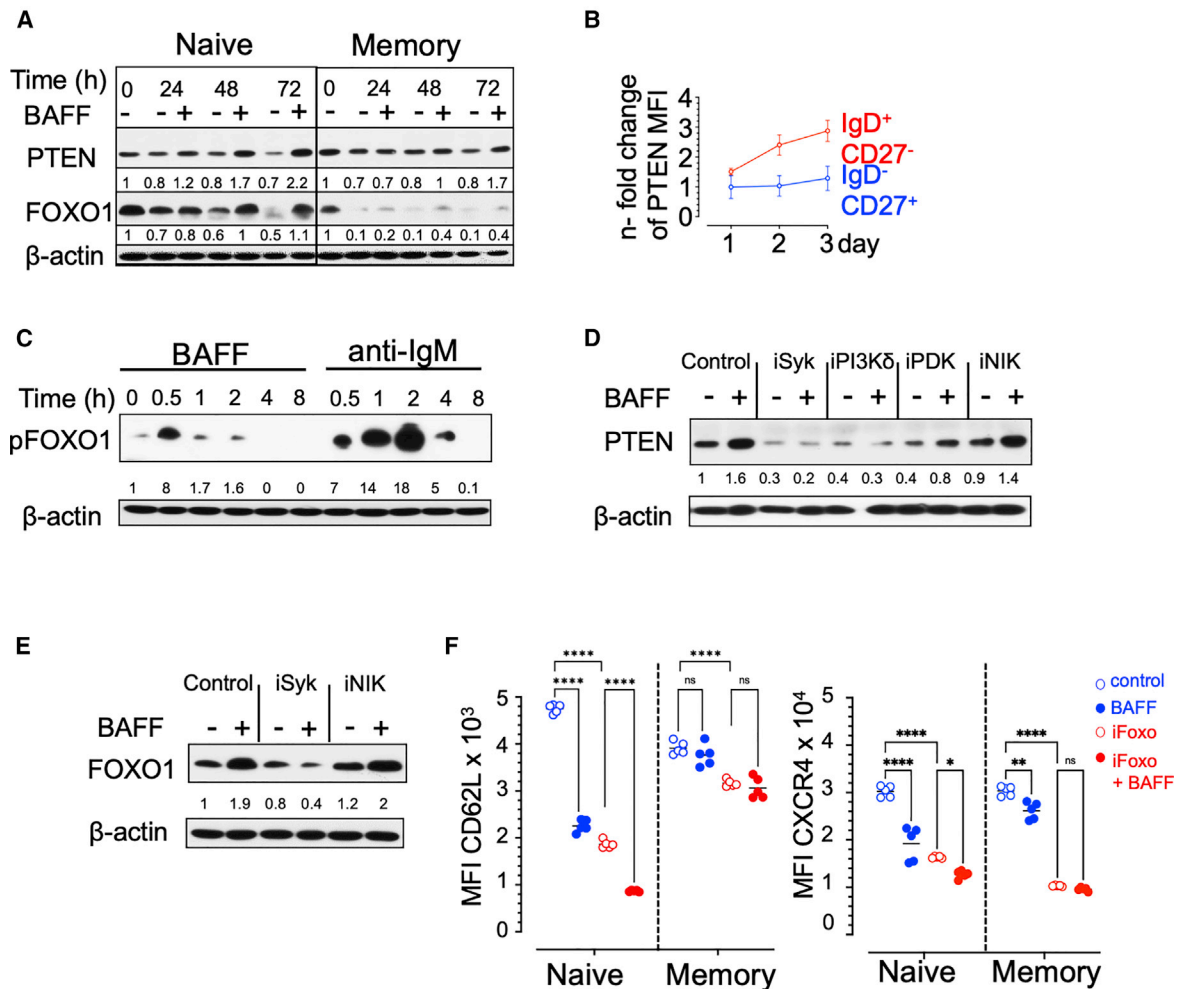


**Figure 4. BAFFR regulates the expression of PTEN and FOXO1**

(A) Western blot analysis of PTEN and FOXO1 in naive and MBCs treated for 24–72 h  $\pm$  BAFF (20 ng/mL). N-fold changes of PTEN and FOXO1 expression were calculated as signals normalized to actin and further normalized to untreated samples from day 0 per subset. The experiment was performed once in this format. (B) Flow cytometric analysis of PTEN expression in naive and MBCs treated for 24–72 h  $\pm$  BAFF. N-fold change of PTEN MFI was calculated as [(PTEN MFI + BAFF)/(PTEN MFI –BAFF)].

(C) Western blot analysis of phosphorylated FOXO1 (S256) in naive B cells treated with BAFF or F(ab)<sub>2</sub> anti-IgM (2  $\mu$ g/mL) for 0.5–8 h. N-fold change in pFOXO1 levels was calculated as described in (A).

(D) Western blot analysis of PTEN in naive B cells treated with inhibitors against SYK (2.5  $\mu$ M R406), PI3K $\delta$  (0.625  $\mu$ M nemiralisib), PDK1 (5  $\mu$ M BX-795), NIK (10  $\mu$ M SMI1), or DMSO (control)  $\pm$  BAFF for 2 days.

(E) Western blot analysis of FOXO1 in naive B cells treated with iSYK, iNIK, or DMSO  $\pm$  BAFF for 2 days.

(D and E) Blots are representative of  $\geq 2$  independent experiments. N-fold changes were calculated as signals normalized to actin and further normalized to the control untreated sample.

(F) Flow cytometric analysis of CD62L and CXCR4 in naive and MBCs treated overnight with BAFF in the presence of FOXO1 inhibitor (2.5  $\mu$ M AS1842856) or DMSO (control). Plots show the mean of CD62L and CXCR4 MFI from 2 independent experiments (2–3 replicates/experiment, 2 HDs). \* $p < 0.05$ ; \*\* $p < 0.01$ ; \*\*\*\* $p < 0.0001$ ; ns, not significant (2-way ANOVA with Tukey multiple comparisons test).

on FOXO1 activity. Like the cultivation in the presence of BAFF, treatment of B cells with a FOXO1 inhibitor reduced CD62L expression on naive B cells by 60%, while their combination resulted in an 80% decrease. This indicates that BAFF controls CD62L expression at least in part through inactivating FOXO1. Likewise, treatment with BAFF or inhibition of FOXO1 also decreased CXCR4 surface levels in naive B cells. BAFF decreased only slightly the expression of CD62L or CXCR4 in MBCs, whereas FOXO1 inhibition led to a much stronger down-

regulation (Figure 4F). Thus, FOXO1 controls the expression of CD62L and CXCR4 in both B cell subsets, whereas BAFF controls their expression only in naive B cells.

#### BAFFR co-localizes with the BCR complex and signals through CD79A/CD79B

Since the activation of BAFFR in naive B cells correlated with the phosphorylation of proteins linked to BCR signaling, we tested whether BAFFR would interact directly with BCR components.

DG-75 Burkitt's lymphoma cells were incubated for different time points with FLAG-tagged BAFF, which was then immunoprecipitated with anti-FLAG beads. Co-immunoprecipitating proteins were analyzed by western blotting using TRAF3 as control (Figure S4A). Since CD79B and the  $\mu$ -heavy chain ( $\mu$ -HC) co-immunoprecipitated together with BAFF and BAFFR from lysates of cells incubated with the ligand on ice, BAFFR seemed to be associated with the BCR before signaling was initiated. After 30 min, the signals of CD79B and  $\mu$ -HC became weaker, suggesting that the complex of BAFFR and the BCR is regulated by BAFF (Figure 5A).

To support these results by an independent approach, we analyzed Förster resonance energy transfer (FRET) from BAFFR-CFP to CD79A- or CD79B-YFP/-RFP fusion proteins. Lentiviral transduction in BAFFR-KO DG-75 cells resulted in mixed populations expressing different combinations of BAFFR-CFP, CD79A-YFP, and CD79B-RFP, or of BAFFR-CFP, CD79B-YFP, and CD79A-RFP (Figures 5B, 5C, and S4B). Because the extracellular domains of CD79A and CD79B are linked by a disulfide bridge, FRET between CD79A-YFP and CD79B-RFP (or CD79B-YFP and CD79A-RFP) served as a positive control, while single positive cells were used to compensate the spillover emission of CFP, YFP, and RFP into the channels detecting FRET-induced fluorescence of YFP or RFP (Figure S4B).

Interactions between BAFFR-CFP and CD79A/CD79B-YFP or CD79A/CD79B-RFP were recorded in the CFP<sup>+</sup> YFP<sup>+</sup> RFP<sup>+</sup> population as the percentage of YFP-FRET<sup>+</sup> or RFP-FRET<sup>+</sup> cells, respectively (Figures 5C and S4B). The analysis revealed that the percentages of CD79B-YFP-FRET<sup>+</sup> or CD79B-RFP-FRET<sup>+</sup> cells were higher than the percentages of CD79A-YFP-FRET<sup>+</sup> or CD79A-RFP-FRET<sup>+</sup> cells (Figure 5D), implying that BAFFR is closer to CD79B than to CD79A. In analogy to the co-immunoprecipitation experiments, activation with BAFF or anti-IgM significantly decreased the percentage of FRET<sup>+</sup> cells (Figure 5D). Thus, BAFFR seemed to form a complex with the BCR by directly interacting with its signaling subunits CD79A and CD79B. FRET signals generated from interactions between BAFFR and CD79A/B were also significantly weaker compared to those between CD79A and CD79B. This could mean that not all BAFFR molecules interact with CD79A/CD79B heterodimers, that the distances are larger, or that the interaction times are shorter. In addition, the interactions between BAFFR and CD79A/CD79B heterodimers became weaker when BAFF was binding to BAFFR, either because the complex had dissociated or because of conformational changes due to the binding of TRAF3 to the cytoplasmic tail of BAFFR (Figure S4A), which may have interfered with the FRET signals.

To determine whether BAFFR required an intact BCR complex to activate PI3K, we inactivated the *CD79A*, *CD79B*, or *IGHM* locus in DG-75 cells (Figure S4C). Loss of any of these proteins prevented AKT phosphorylation in response to BAFF (Figures 5E and 5F) or anti-IgM (Figure S4D), whereas activation of NF- $\kappa$ B2 did not change (Figure S4E). In primary B cells, inactivation of *CD79A* and *CD79B* severely reduced cell numbers over a 5-day cultivation period showing the strong dependence of naive and MBCs on the expression of functional BCRs (Figures S4F and S4G). Since the inactivation of *CD79A* in primary B cells was not as efficient as the inactivation of *CD79B*, some of the

naive B cells in the CD79A KO samples were rescued by BAFF (Figure S4G). Hence, the survival of human B cells strongly depends on the expression of the BCR components CD79A and CD79B, which serve as signaling partners of BAFFR to activate the PI3K pathway.

### Ig isotypes regulate BAFFR-BCR interactions and BAFF-induced activation of PI3K

Since BAFF activated PI3K signaling in IgM<sup>+</sup> IgD<sup>+</sup> naive B cells, but not in IgG<sup>+</sup> or IgA<sup>+</sup> MBCs, and as the activation of PI3K required interactions between BAFFR and the BCR, we tested if the isotype switch from IgM/IgD to IgG or IgA would change BAFFR-BCR interactions.

As the weak response of MBCs to BAFF could be related to the number of BCRs on their surface, we analyzed the surface expression of their BCRs using the expression of Ig- $\kappa$  and  $\lambda$  light chains as reference. Compared to naive B cells, IgA<sup>+</sup> and IgG<sup>+</sup> MBCs had fewer light chains on the cell surface (Figures 6A and S5A), which correlated with the lower surface expression of CD79A and CD79B, whereas their intracellular levels were similar in both subsets (Figure 6B).

To determine whether different immunoglobulin isotypes would alter BAFF-induced AKT activation, we used DG-75 cells expressing IgM, IgD, IgA, or IgG as a model. These lines were constructed by first inactivating the endogenous  $\mu$ -HC locus (*IGHM*). IgG1 and IgA1 expressing variants were then generated by lentiviral gene transfer of SARS-CoV-2 Spike protein-specific IgA1 or IgG1 into the  $\mu$ -HC knockout (KO) cells (Figures S5B and S5C). The IgD<sup>+</sup> line developed fortuitously from the  $\mu$ -HC KO line, most likely by differential splicing of the long VDJ-C $\mu$ -C $\delta$  pre-mRNA transcript. BAFFR and CD19 expression was similar in all of the cell lines, whereas CD79B levels were lower in the IgA and IgD lines (Figure S5B).

Activation with BAFF resulted in similar kinetics of AKT phosphorylation in the IgM<sup>+</sup> and in the IgD<sup>+</sup> cells, whereas it was weaker and slower in the IgA<sup>+</sup> and the IgG<sup>+</sup> lines (Figure 6C). Processing of NF- $\kappa$ B2 and TRAF3 recruitment remained unchanged (Figures S5D and S5E), and BCR activation induced strong AKT phosphorylation for all isotypes (Figure S5F). The weaker phosphorylation of AKT in the IgA<sup>+</sup> or IgG<sup>+</sup> cells was not related to the lentiviral gene transfer of these BCRs, as BAFF induced a similar pattern of AKT phosphorylation in DG-75  $\mu$ -HC KO or IgD<sup>+</sup> cells reconstituted with the SARS-CoV-2 Spike-specific IgM as in parental IgM<sup>+</sup> DG-75 cells (Figure S5G).

As BAFFR was found to interact with IgM BCRs on DG-75 cells (Figure 5), we used the FRET-based approach to examine whether different Ig isotypes would change these interactions. IgM-, IgD-, IgA-, or IgG-expressing BAFFR KO DG-75 cells were transduced with vectors encoding BAFFR-CFP and CD79A- and CD79B-YFP or -RFP fusion proteins. Compared to the IgM and IgD lines, the percentage of FRET<sup>+</sup> cells resulting from interactions between BAFFR-CFP and CD79A or CD79B YFP dropped from 15%–17% to 11% for IgG and to 13% for IgA lines (Figure 6D). Binding of BAFF to BAFFR reduced the percentage of FRET<sup>+</sup> cells expressing IgM by 20%, whereas the IgD, IgG, or IgA lines showed a similar or smaller decrease in FRET<sup>+</sup> cells in response to BAFF (Figure 6D).

These results imply that BAFFR interacts best with IgM, followed by IgD, IgA, and IgG. Therefore, the combination of low TCL1A

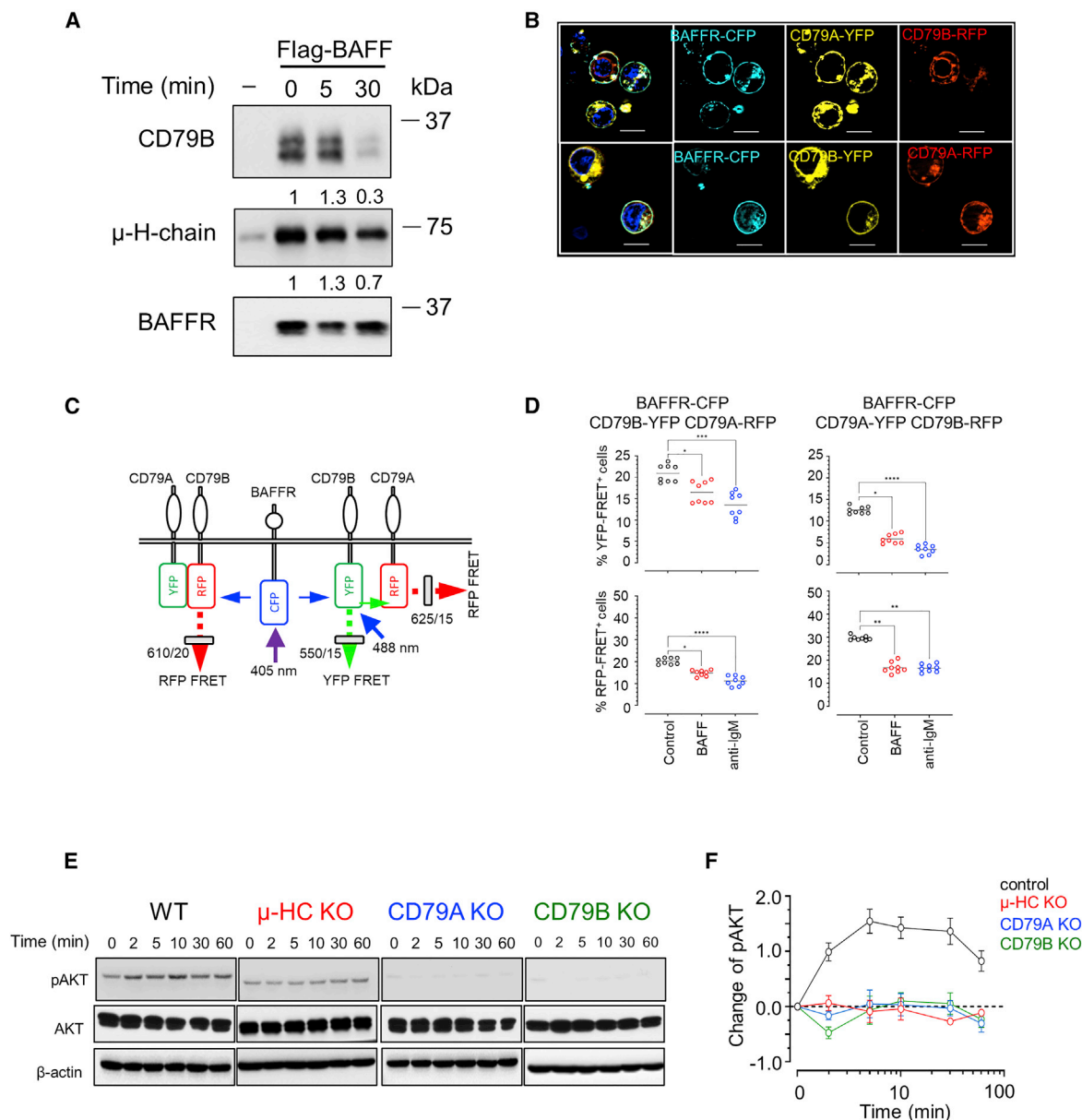


**Figure 5. BAFFR co-localizes with the BCR complex and signals through CD79A/CD79B**

(A) DG-75 cells were incubated for 0–30 min with FLAG-tagged BAFF followed by co-immunoprecipitation with anti-FLAG M2 agarose beads and western blot analysis for CD79B, μ-HC, and BAFFR. Immunoprecipitates of untreated cells (–) were used as controls for unspecific binding. N-fold changes were calculated as signals normalized to BAFFR and further normalized to t = 0 sample.

(B) Immunofluorescence of DG-75 cells expressing BAFFR-CFP and CD79A- and CD79B-YFP or -RFP. Nuclei were stained with Hoechst 33342 (blue). Scale bars, 10 μm.

(C) Schematic representation of FRET analysis. BAFFR-CFP emission excited by the 405-nm laser induces FRET-based excitation of YFP and RFP fused to CD79A or CD79B. FRET from CFP to YFP is detected as YFP emission with a 550/15-nm BP filter, and FRET from CFP to RFP is detected as RFP emission with a 610/20-nm BP filter. FRET from YFP excited by the 488-nm laser to RFP is detected by a 625/15-nm BP filter. Excitations are shown by solid arrows, emissions by dashed arrows.

(D) Percentage of FRET<sup>+</sup> cells in DG-75 cells expressing BAFFR-CFP and CD79A- and CD79B-YFP or -RFP incubated with BAFF (100 ng/mL) or F(ab)<sub>2</sub> anti-IgM (2 μg/mL) or left untreated (control) for 6 h. Plots show the mean of 2 independent experiments (4 technical replicates per experiment). \*p < 0.05; \*\*p < 0.01; \*\*\*p < 0.001; \*\*\*\*p < 0.0001 (Kruskal-Wallis with Dunn's multiple comparisons test).

(E and F) Western blot analysis of pAKT and AKT in WT, CD79A, CD79B, or μ-HC KO DG-75 cells treated with BAFF for 2–60 min. (F) pAKT signals as shown in (E) were normalized to actin and changes in pAKT values were calculated as [(signal t<sub>x</sub> – signal t<sub>0</sub>)/signal t<sub>0</sub>]. Data are shown as means ± SEMs of ≥ 5 independent experiments.

See also Figure S4.

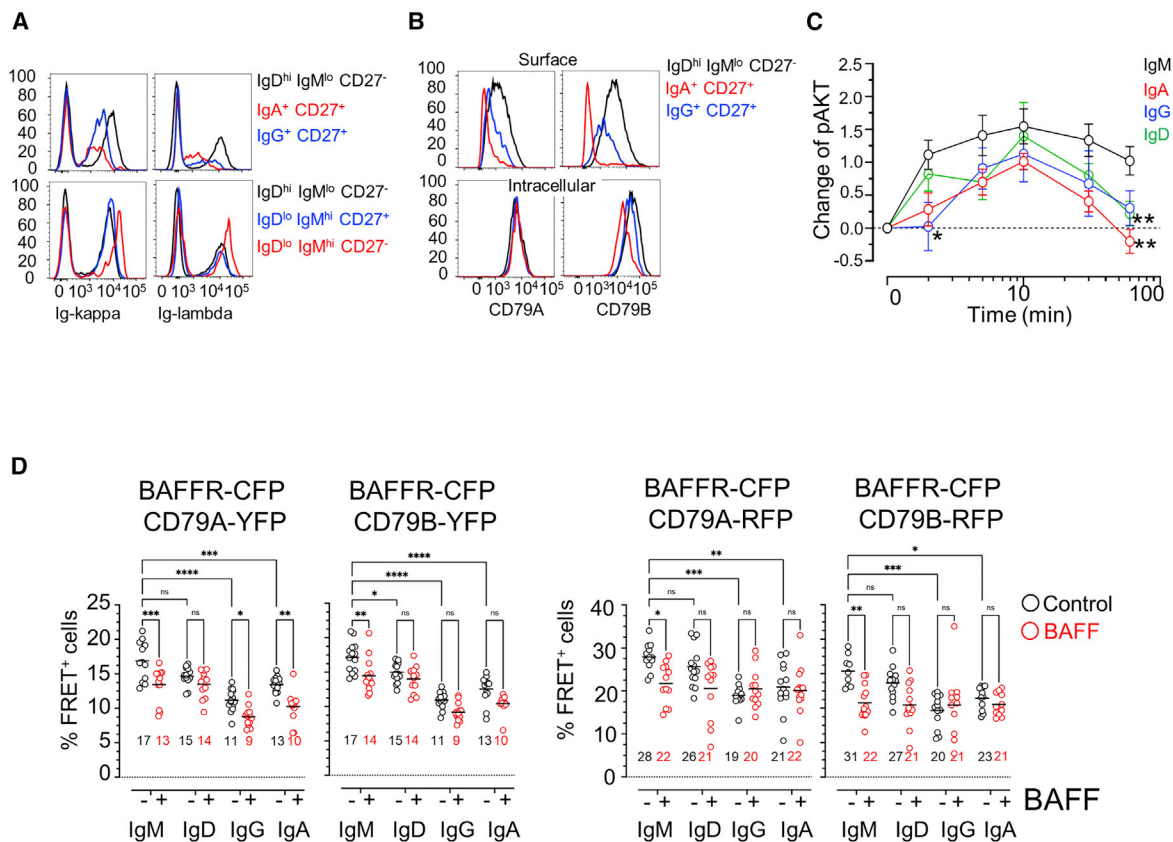


**Figure 6. Immunoglobulin isotypes regulate BAFFR-BCR interactions and BAFF-induced activation of PI3K**

(A) Flow cytometric analysis of Ig- $\kappa$  and Ig- $\lambda$  L-chains expression in IgD<sup>hi</sup> IgM<sup>lo</sup> CD27<sup>-</sup> naive, IgD<sup>lo</sup> IgM<sup>hi</sup> CD27<sup>+</sup> MZ, IgD<sup>lo</sup> IgM<sup>hi</sup> CD27<sup>-</sup>, IgA<sup>+</sup> CD27<sup>+</sup>, and IgG<sup>+</sup> CD27<sup>+</sup> MBCs. See also Figure S5A.

(B) Similar to (A), showing surface and intracellular expression of CD79A and CD79B.

(C) Changes in pAKT values analyzed by western blot in DG-75 cells expressing IgM, IgD, IgA1, or IgG1 treated with BAFF (100 ng/mL) for 2–60 min, calculated as [(signal t<sub>x</sub> – signal t<sub>0</sub>)/signal t<sub>0</sub>]. pAKT signals were previously normalized to actin. Plot shows the means  $\pm$  SEMs of  $\geq 4$  independent experiments. \*p < 0.05; \*\*p < 0.01 (Mann-Whitney test).

(D) Percentage of FRET<sup>+</sup> cells in IgM<sup>+</sup>, IgD<sup>+</sup>, IgA1<sup>+</sup>, or IgG1<sup>+</sup> DG-75 cells expressing BAFFR-CFP and CD79A- and CD79B-YFP or -RFP treated with BAFF or left untreated (control) for 6 h. The percentage of FRET<sup>+</sup> cells was determined as outlined in Figures 5C and S4B. Plots show the mean of 3 independent experiments (3–4 technical replicates). \*p < 0.05; \*\*p < 0.01; \*\*\*p < 0.001; \*\*\*\*p < 0.0001 (2-way ANOVA with Tukey multiple comparisons test). See also Figure S5.

expression, less BCRs on the surface of IgG<sup>+</sup> or IgA<sup>+</sup> MBCs, and weaker interactions between BAFFR and IgG or IgA BCRs could reduce BAFFR signaling strength below a threshold level that has to be reached to activate PI3K signaling in response to BAFF.

### BAFFR inactivation impairs survival of naive and of MBCs

To determine if BAFFR has any other function in MBCs, we inactivated the *BAFFR* gene by CRISPR-Cas9 mutagenesis in primary B cells. To assess the effect of gene targeting by electroporation on cell survival, we also inactivated *CD27* as it is transcribed in MBCs and it is easily detected by flow cytometry (Figures S6A–S6C). Compared to mock electroporated cells, the loss of *CD27* reduced the numbers of IgD<sup>+</sup> naive and MZ B cells by 30% (Figure 7A). However, inactivation of *BAFFR* decreased the numbers of naive and MBCs by >50%–60% (Figure 7A), which was comparable to the KO of *CD79A* and *CD79B* (Figure S4G). As expected, cultiva-

tion with BAFF did not improve the survival of B cells after the loss of BAFFR, while BAFF was still able to rescue naive B cells from cell death in the *CD27* KO (Figure 7B). Although MBCs express *TACI*, which also binds BAFF and could thus limit BAFFR-induced functions, gene inactivation of *TACI* did not improve their survival in response to BAFF (Figure S6D).

In summary, we conclude that BAFFR seems to have different functions in human B cells. In transitional B cells, BAFFR has critical pro-survival activities that allow the development of the MZ and of naive follicular B cells (Warnatz et al., 2009). In naive B cells, BAFFR-BCR interactions activate PI3K- and NF- $\kappa$ B2-associated signaling reactions, which regulate a variety of cellular functions, ranging from survival to cell migration. In both naive B cells and MBCs, BAFFR seems to be a structural component of a BCR-associated protein complex, which must remain intact to ensure the survival of these subsets.

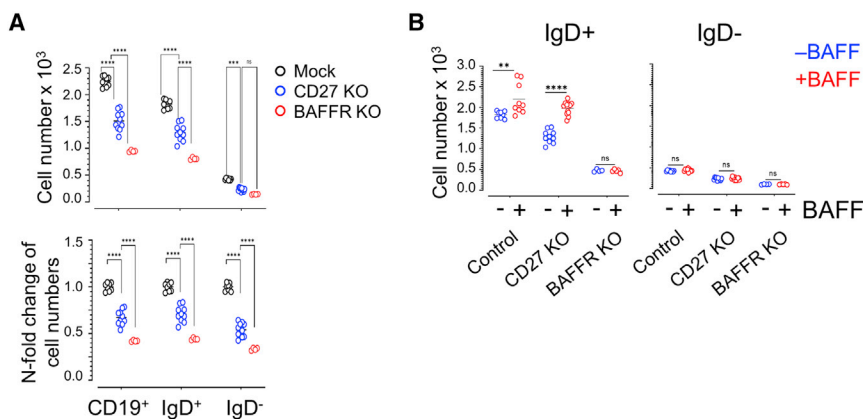


**Figure 7. BAFFR inactivation impairs survival of naive and MBCs**

(A) (Top) Cell numbers of B cell subsets (IgD<sup>+</sup>: naive and MZ; IgD<sup>-</sup>: MBCs) analyzed by flow cytometry and timed acquisition 5 days post-electroporation with guide RNA (gRNA)/Cas9 RNPs against *BAFFR* and *CD27* or without RNP (mock). (Bottom) N-fold changes were calculated as (cell number of KO)/(cell numbers of mock). \*\*\**p* < 0.001; \*\*\*\**p* < 0.0001; ns, not significant (2-way ANOVA with Tukey multiple comparisons test).

(B) *BAFFR* and *CD27* were inactivated in B cells as shown in (A). Two days post-electroporation, cells were treated  $\pm$  BAFF (20 ng/mL) for 3 days and cell numbers were analyzed by flow cytometry and timed acquisition; in the

BAFFR KO, only the BAFFR-low population was evaluated. \*\**p* < 0.01; \*\*\*\**p* < 0.0001; ns, not significant (2-way ANOVA with Sidak's multiple comparisons test).

(A and B) Plots show the mean from 2 independent experiments ( $\geq 2$  technical replicates, 2 HDs).

## DISCUSSION

BAFFR, B cell maturation antigen (BCMA), and their ligands BAFF and APRIL have been described as essential survival factors for B cells and plasma cells (Mackay and Schneider, 2009; O'Connor et al., 2004; Yeh et al., 2020). However, human MBCs, which express as much BAFFR as naive B cells, survive for months, if not years, without BAFF or APRIL (Jacobi et al., 2010; van Vollenhoven et al., 2011). Since human naive B cells require BAFFR for survival (Warnatz et al., 2009), we wondered whether BAFFR signaling responses would differ between naive and MBCs. Here, we report that BAFF activates the PI3K pathway in naive B cells but not in MBCs.

By dissecting BAFF-induced signaling and the interactions between BAFFR and the BCR, we found by two lines of evidence that Ig isotypes determine the quality of the interactions between BAFFR and the BCR components CD79A/B, which are required by BAFFR to activate PI3K signaling. First, IgG<sup>+</sup> and IgA<sup>+</sup> MBCs express fewer BCRs and less CD79A/B on their surface than naive B cells. Second, our FRET analyses revealed weaker interactions between BAFFR and CD79A/CD79B in cell lines expressing IgA or IgG BCRs compared to those with IgM and IgD. Since CD79A and CD79B are needed to activate PI3K signaling in response to BAFF, the combination of fewer BCRs with weaker BAFFR-BCR interactions could suffice to prevent BAFF-induced PI3K activation.

BAFFR-CFP had to be located closer than 10 nm to the CD79A- and CD79B-YFP or -RFP fusion proteins to allow FRET-based emission of yellow or red light from YFP or RFP through the excitation of CFP (Schneider et al., 2014). As the minimal distance between the CFP, YFP, and RFP fluorochromes is  $\geq 3$  nm, BAFFR and CD79A or CD79B must be in close proximity, if not in direct contact. The interaction interfaces between BAFFR and CD79A/B are unknown, but they may involve the transmembrane (TM) regions, which also promote the association between CD79A, CD79B, and the  $\mu$ -HC (Dylke et al., 2007; Reth, 1992). BAFF binding reduced BAFFR/BCR interactions, and this decrease was correlated with TRAF3 recruitment to the C-terminal end of BAFFR, indic-

ative of a major rearrangement of the BAFFR/BCR complex. These changes remind one of the receptor-dissociation model (Yang and Reth, 2010), according to which antigen binding leads to the opening of a densely packed complex consisting of several BCRs (Klasener et al., 2014). In any case, BAFF-induced PI3K activation requires an intact BCR, as the loss of the  $\mu$ -H chain of CD79A or CD79B prevented BAFF-induced AKT phosphorylation.

Rapid activation of the BCR-associated SRC kinase LYN was one of the first steps in PI3K activation following BAFF binding. After a short burst, LYN activation was shut down again as indicated by the strong phosphorylation of the inhibitory Y508 detected 30 min after adding BAFF. The activation of LYN was followed by the phosphorylation of SYK, CD79A, and CD19 in a very similar way as it has been observed in mouse B cells (Jellusova et al., 2013; Otipoby et al., 2008; Patke et al., 2006; Schweighoffer et al., 2013; Woodland et al., 2008). These initial signaling events led in naive B cells to the upregulation of BCL-2, BCL-XL, and MCL1. On the contrary, resting MBCs expressed 1.5–3 times higher levels of all three anti-apoptotic proteins, which could contribute to their longevity.

In addition to these anti-apoptotic factors, BAFF binding in naive B cells changed within 6 h the transcription of >300 functionally related genes coding for chemokines, interleukins, and their receptors. By producing chemokines and interleukins such as IL-6 and IL-1 $\beta$ , BAFF-stimulated naive B cells would acquire the potential to activate neutrophils, which can produce more BAFF and secrete IL-21 (Puga et al., 2011). By upregulating IL-21R in naive B cells, BAFF in combination with IL-21 promoted their proliferation but not that of MBCs. This result contradicts a previous report showing that BAFF and IL-21 induce the proliferation of human splenic IgG1 MZ but not follicular B cells (Ettinger et al., 2007). However, circulating B cells analyzed in our study may differ in their response to BAFF from tissue-resident cells. As according to CD69 and CD83 expression, BAFF activated under optimal condition 50%–80% of peripheral naive B cells, it can be speculated that circulating naive B cells may fall into two groups, one that responds to BAFF and another that does

not. The latter may contain B cells of the population described by Ettinger et al. (2007).

By downregulating S1PR1, CD62L, and CXCR4 expression, BAFF controls the migration pattern of naive B cells. S1PR1 regulates the entry of murine and human B cells into circulation along an S1P gradient (Cinamon et al., 2004; Sic et al., 2014). Since S1PR1 activity is directly blocked by CD69 (Bankovich et al., 2010; Shioh et al., 2006), which was strongly upregulated by BAFF, BAFF-activated naive B cells stopped migrating in response to S1P. BAFFR ligation in naive B cells also reduced the surface expression of CD62L and CXCR4 through the suppression of the FOXO1 transcriptional activity. These findings are in line with previous studies showing that FOXO1 modulates peripheral B cell homing and the formation of dark zone within the GCs through the upregulation of CD62L (Dengler et al., 2008) and CXCR4 (Dominguez-Sola et al., 2015; Sander et al., 2015). Thus, BAFFR-derived signals could synergize with chemokines and integrins to control the rolling, adhesion, and positioning of naive B cells within the follicles.

As PTEN counteracts the activity of PI3K by dephosphorylating PIP3, high PTEN expression levels in MBCs may have explained the weak activation of the pathway by BAFF. However, PTEN levels were comparable between naive and MBCs, while BAFF gradually upregulated PTEN expression in naive B cells through the PI3K pathway like in mouse B cells (Patke et al., 2006). Since FOXO1 positively regulates PTEN levels while PTEN maintains the activity of FOXO1 by blocking PI3K (Hawse et al., 2015; Park et al., 2019), BAFF may use this feedback loop to downregulate BAFFR signaling in naive B cells.

In contrast to PTEN, which antagonizes PI3K and limits the activation of downstream substrates such as AKT, TCL1A acts as a co-activator of AKT (Laine et al., 2000; Pekarsky et al., 2000) and its deregulated expression has been linked with lymphomagenesis (Bichi et al., 2002; Herling et al., 2007, 2009; Pekarsky et al., 2008). As human naive B cells were found to express 25–30 times more TCL1A than MBCs, we therefore thought that this difference may be sufficiently large to explain why PI3K signaling is activated by BAFF in naive B cells but not in MBCs. Inactivation of *TCL1A* in DG-75 cells partially reduced BAFF-dependent AKT phosphorylation, while in naive B cells, it interfered with the BAFF-induced upregulation of CD69, which depends on PI3K activity. This suggests that high TCL1A expression levels in naive B cells enhance BAFF-induced AKT activity, whereas low TCL1A levels in MBCs may contribute to their unresponsiveness to BAFF. As loss of TCL1A did not reduce BAFF-dependent survival, it could be speculated that activation of NF- $\kappa$ B2, which does not depend on PI3K/AKT, could have supported the survival of TCL1A KO naive B cells. However, these differences in TCL1A expression levels seem not to account for the different needs of naive B cells and MBCs for BAFF as a pro-survival factor.

Different from induction of PI3K signaling, BAFF activated NF- $\kappa$ B2 not only in naive B cells but also in MBCs. However, only the survival of naive B cells was sensitive to NIK inhibition due to the downregulation of BCL-2. Therefore, BAFF-induced NF- $\kappa$ B2 activity may have different functions in MBCs than in naive B cells.

Although BAFFR is expressed at high levels on the surface of MBCs, our data provide strong evidence that it responds only weakly to BAFF and has little or no BAFF-dependent pro-survival function. Two recent reports, however, reported that BAFFR is required to generate unmutated MBCs in extrafollicular B cell responses (Lau et al., 2020) as well as for the survival of MBCs (Müller-Winkler et al., 2021). Different from human MBCs, mouse MBCs responded to BAFF as well as naive B cells, and the depletion of BAFF impaired MBC survival and antibody recall responses (Müller-Winkler et al., 2021). Although immunophenotypic studies of belimumab-treated SLE patients (Jacobi et al., 2010; Stohl et al., 2012) and our own data strongly suggest that human MBCs do not require BAFF/BAFFR-induced responses for survival, we show that, at least *in vitro*, the survival of MBCs depends on BAFFR expression. In fact, inactivation of the *BAFFR* locus affected the survival of human B cells *in vitro* almost as strongly as the inactivation of *CD79A* or *CD79B*, which is in line with the findings for MBCs made in mice (Müller-Winkler et al., 2021). As BAFFR assembles with the BCR into a larger complex, which is required for BCR signaling in mice (Keppler et al., 2015; Mattila et al., 2013), loss of BAFFR, *CD79A*, or *CD79B* may disrupt the complex and lead to cell death. Accordingly, BAFFR would have structural functions in MBCs that would not depend on its BAFF-induced activity.

As MBCs also express TACI, which binds and responds to oligomeric BAFF and APRIL (Bossen et al., 2008), TACI-induced pro-survival signals could replace BAFFR signals. However, TACI levels are significantly lower than BAFFR due to its constitutive shedding from the surface by ADAM10 (Hoffmann et al., 2015). If BAFF is limiting, one could assume that high BAFFR expression levels on MBCs would compete with low TACI levels for BAFF binding and reduce TACI-dependent signals and pro-survival functions. Since TACI also binds APRIL, the cytokine could replace BAFF in patients treated with BAFF-neutralizing antibodies. However, treatment of rheumatoid arthritis patients with soluble TACI-Fc (atacept, which also neutralized APRIL) led to a similar reduction in naive B cells but spared MBCs (Tak et al., 2008; van Vollenhoven et al., 2011). TACI also has, like BAFFR, *CD79A*, and *CD79B*, a ligand-independent function, as recently shown by us, because its overexpression in human B cells strongly supports TLR9-dependent proliferation, while its inactivation impairs the survival and proliferation of B cells (Smulski et al., 2022). Therefore, BAFF- (and APRIL-) independent survival of MBCs could depend on tonic signals induced by the expression of BAFFR and TACI.

In conclusion, the combination of at least three factors seems to regulate the differential response of naive B cells and MBCs to BAFF. One important factor is the interactions between BAFFR and the BCR components *CD79A* and *CD79B*, as the nature of these interactions seems to depend on the Ig isotype. Different BCR expression levels in naive and MBCs seem to be the second factor, as they are low in MBCs and high in naive B cells. The combination of both factors sets probably the threshold for BAFFR activation in naive B cells and MBCs, which seems to be modulated in addition by the AKT coactivator TCL1A that is highly expressed in naive B cells but not in MBCs. In naive human B cells, the activation of BAFFR rapidly changes the transcription of hundreds of genes regulating survival, protein

synthesis, migration, activation, and cell-cell interactions. Thus, BAFF-induced signals regulate many aspects of naive B cell fate, while the longevity of MBCs requires the functional interactions between BAFFR and the BCR.

### Limitations of the study

Although we tried to analyze the functional consequences of BAFF/BAFFR interaction in naive and MBCs as thoroughly as possible, our study has some obvious limitations. First, many of the functional analyses were based on *in vitro* approaches using human B cells isolated from peripheral blood. CRISPR-Cas9-mediated gene inactivation of *CD79A*, *CD79B*, *BAFFR*, and *CD27*, for instance, was achieved by electroporation, which kills approximately 50% of the cells and induces stress in the surviving cells. It is therefore not unlikely that electroporation-induced stress adds up to the effects caused by the inactivation of the respective genes. Moreover, the CRISPR-Cas9-induced inactivation of genes in resting human B cells does not lead to the immediate loss of the corresponding proteins and it does not occur equally in all cells, although almost all cells uptake ribonucleoprotein (RNP) complexes. This leaves a “background” of cells that still express the genes that were targeted. Therefore, the effects observed *in vitro* may not exactly reflect the loss of BAFFR, *CD79A*, *CD79B*, or *CD27* function in human B cells *in vivo*. In spite of these limitations, our results are in line with those of the conditional inactivation of BAFFR in mature B cells in mice.

Second, some of the experiments analyzing BAFFR-BCR interactions were performed in human B cell lines transduced with different lentiviral expression vectors; and third, the RNA-seq transcriptome analysis of resting and BAFF-activated B cells was performed on isolated B cells cultivated *in vitro* for 6 h. It should, however, be considered that functional *in vivo* cause-relation analyses of human B cells are very difficult if not impossible, apart from, for example, infection, vaccination, or transplantation experiments.

Therefore, most *ex vivo* analyses of human B cells were and are snapshots of single moments, and in the case of functional studies, influenced by experimentation. Other *in vivo* models such as humanized mice provide only limited insight into a small time window and do not allow the analysis of long-lived MBCs (Lang et al., 2017), which would leave only closely related primates as model systems to study the role of BAFFR in maintaining long-lived MBCs. Such studies have in fact been carried out and support the view that primate MBCs are much less dependent on BAFF/BAFFR signaling than murine MBCs (Borhis et al., 2020; Lin et al., 2007; Vugmeyster et al., 2006).

### STAR★METHODS

Detailed methods are provided in the online version of this paper and include the following:

- KEY RESOURCES TABLE
- RESOURCE AVAILABILITY
  - Lead contact
  - Materials availability
  - Data and code availability

### ● EXPERIMENTAL MODEL AND SUBJECT DETAILS

- Primary cells and cell lines

### ● METHOD DETAILS

- Plasmids, transfection and transduction
- Isolation of B cells
- *In vitro* activation and inhibition of cells
- Flow cytometry
- Western blot analysis
- Co-immunoprecipitation
- Flow cytometry-based FRET
- RNA extraction and RNA sequencing
- Assembly of the ribonucleoprotein (RNP) complexes and electroporation of cells

### ● QUANTIFICATION AND STATISTICAL ANALYSIS

### SUPPLEMENTAL INFORMATION

Supplemental information can be found online at <https://doi.org/10.1016/j.celrep.2022.111019>.

### ACKNOWLEDGMENTS

This work has been supported by the DFG to project P06 of H.E. within the collaborative research center TRR130, and the DFG grant Ei235/9-1 to H.E. P.S. is supported by the Swiss National Science Foundation (31003A-176256). The computational RNA-seq analysis was performed using the resources of Friedrich Schiller University Jena, supported in part by DFG grants INST 275/334-1 FUGG and INST 275/363-1 FUGG.

### AUTHOR CONTRIBUTIONS

Conceptualization, H.E.; methodology, E.S. and H.E.; investigation, E.S., V.B., M.L., M.H., H.L., C.R.S., J.-S.B., Y.H., B.F., and N.-J.R.; writing – original draft, E.S. and H.E.; writing – review & editing, E.S., V.B., M.L., C.R.S., J.-S.B.; N.-J.R., B.G., H.-M.J., R.E.V., M.H., P.S., and H.E.; funding acquisition, M.H., P.S., and H.E.; resources, C.R.S., B.G., H.-M.J., R.E.V., M.H., P.S., and H.E.; supervision, H.E.

### DECLARATION OF INTERESTS

The authors declare no competing interests.

Received: December 3, 2021

Revised: April 27, 2022

Accepted: June 8, 2022

Published: June 28, 2022

### REFERENCES

- Bankovich, A.J., Shiow, L.R., and Cyster, J.G. (2010). CD69 suppresses sphingosine 1-phosphate receptor-1 (S1P1) function through interaction with membrane helix 4. *J. Biol. Chem.* 285, 22328–22337. <https://doi.org/10.1074/jbc.m110.123299>.
- Bichi, R., Shinton, S.A., Martin, E.S., Koval, A., Calin, G.A., Cesari, R., Russo, G., Hardy, R.R., and Croce, C.M. (2002). Human chronic lymphocytic leukemia modeled in mouse by targeted TCL1 expression. *Proc. Natl. Acad. Sci. USA* 99, 6955–6960. <https://doi.org/10.1073/pnas.102181599>.
- Borhis, G., Trovato, M., Ibrahim, H.M., Isnard, S., Le Grand, R., Bosquet, N., and Richard, Y. (2020). Impact of BAFF blockade on inflammation, germinal center reaction and effector B-cells during acute SIV infection. *Front. Immunol.* 11, 252. <https://doi.org/10.3389/fimmu.2020.00252>.
- Bossen, C., Cachero, T.G., Tardivel, A., Ingold, K., Willen, L., Dobles, M., Scott, M.L., Maquelin, A., Belnoue, E., Siegrist, C.A., et al. (2008). TACI, unlike BAFF-R, is solely activated by oligomeric BAFF and APRIL to support survival

- of activated B cells and plasmablasts. *Blood* 111, 1004–1012. <https://doi.org/10.1182/blood-2007-09-110874>.
- Cancro, M.P. (2009). Signalling crosstalk in B cells: managing worth and need. *Nat. Rev. Immunol.* 9, 657–661. <https://doi.org/10.1038/nri2621>.
- Chen, J., Limon, J.J., Blanc, C., Peng, S.L., and Fruman, D.A. (2010). Foxo1 regulates marginal zone B-cell development. *Eur. J. Immunol.* 40, 1890–1896. <https://doi.org/10.1002/eji.200939817>.
- Chen, K., Coonrod, E.M., Kumánovics, A., Franks, Z.F., Durtschi, J.D., Margraf, R.L., Wu, W., Heikal, N.M., Augustine, N.H., Ridge, P.G., et al. (2013). Germline mutations in NFKB2 implicate the noncanonical NF- $\kappa$ B pathway in the pathogenesis of common variable immunodeficiency. *Am. J. Hum. Genet.* 93, 812–824. <https://doi.org/10.1016/j.ajhg.2013.09.009>.
- Chen, S., Zhou, Y., Chen, Y., and Gu, J. (2018). fastp: an ultra-fast all-in-one FASTQ preprocessor. *Bioinformatics* 34, i884–i890. <https://doi.org/10.1093/bioinformatics/bty560>.
- Cinamon, G., Matloubian, M., Lesneski, M.J., Xu, Y., Low, C., Lu, T., Proia, R.L., and Cyster, J.G. (2004). Sphingosine 1-phosphate receptor 1 promotes B cell localization in the splenic marginal zone. *Nat. Immunol.* 5, 713–720. <https://doi.org/10.1038/ni1083>.
- Claudio, E., Brown, K., Park, S., Wang, H., and Siebenlist, U. (2002). BAFF-induced NEMO-independent processing of NF- $\kappa$ B in maturing B cells. *Nat. Immunol.* 3, 958–965. <https://doi.org/10.1038/ni842>.
- Cremasco, V., Woodruff, M.C., Onder, L., Cupovic, J., Nieves-Bonilla, J.M., Schildberg, F.A., Chang, J., Cremasco, F., Harvey, C.J., Wucherpfennig, K., et al. (2014). B cell homeostasis and follicle confines are governed by fibroblastic reticular cells. *Nat. Immunol.* 15, 973–981. <https://doi.org/10.1038/ni.2965>.
- Darce, J.R., Arendt, B.K., Wu, X., and Jelinek, D.F. (2007). Regulated expression of BAFF-binding receptors during human B cell differentiation. *J. Immunol.* 179, 7276–7286. <https://doi.org/10.4049/jimmunol.179.11.7276>.
- Dengler, H.S., Baracho, G.V., Omori, S.A., Bruckner, S., Arden, K.C., Castrillon, D.H., DePinho, R.A., and Rickert, R.C. (2008). Distinct functions for the transcription factor Foxo1 at various stages of B cell differentiation. *Nat. Immunol.* 9, 1388–1398. <https://doi.org/10.1038/ni.1667>.
- Di Tommaso, P., Chatzou, M., Floden, E.W., Barja, P.P., Palumbo, E., and Notredame, C. (2017). Nextflow enables reproducible computational workflows. *Nat. Biotechnol.* 35, 316–319. <https://doi.org/10.1038/nbt.3820>.
- Dominguez-Sola, D., Kung, J., Holmes, A.B., Wells, V.A., Mo, T., Basso, K., and Dalla-Favera, R. (2015). The FOXO1 transcription factor instructs the germinal center dark zone program. *Immunity* 43, 1064–1074. <https://doi.org/10.1016/j.immuni.2015.10.015>.
- Dylke, J., Lopes, J., Dang-Lawson, M., Machtaler, S., and Matsuuchi, L. (2007). Role of the extracellular and transmembrane domain of Ig- $\alpha/\beta$  in assembly of the B cell antigen receptor (BCR). *Immunol. Lett.* 112, 47–57. <https://doi.org/10.1016/j.imlet.2007.06.005>.
- Ettinger, R., Sims, G.P., Robbins, R., Withers, D., Fischer, R.T., Grammer, A.C., Kuchen, S., and Lipsky, P.E. (2007). IL-21 and BAFF/BLyS synergize in stimulating plasma cell differentiation from a unique population of human splenic memory B cells. *J. Immunol.* 178, 2872–2882. <https://doi.org/10.4049/jimmunol.178.5.2872>.
- Fabre, S., Carrette, F., Chen, J., Lang, V., Semichon, M., Denoyelle, C., Lazar, V., Cagnard, N., Dubart-Kupperschmitt, A., Mangeney, M., et al. (2008). FOXO1 regulates L-Selectin and a network of human T cell homing molecules downstream of phosphatidylinositol 3-kinase. *J. Immunol.* 181, 2980–2989. <https://doi.org/10.4049/jimmunol.181.5.2980>.
- Furie, R.A., Wallace, D.J., Aranow, C., Fettiplace, J., Wilson, B., Mistry, P., Roth, D.A., and Gordon, D. (2018). Long-Term safety and efficacy of belimumab in patients with systemic lupus erythematosus: a continuation of a seventy-six-week phase III parent study in the United States. *Arthritis Rheumatol.* 70, 868–877. <https://doi.org/10.1002/art.40439>.
- Gaul, B.S., Harrison, M.L., Geahlen, R.L., Burton, R.A., and Post, C.B. (2000). Substrate recognition by the lyn protein-tyrosine kinase. *J. Biol. Chem.* 275, 16174–16182. <https://doi.org/10.1074/jbc.m909044199>.
- Gerst, R., and Hölzer, M. (2019). PCAGO: An interactive tool to analyze RNA-Seq data with principal component analysis. Preprint at bioRxiv. <https://doi.org/10.1101/433078>.
- Gross, J.A., Johnston, J., Mudri, S., Enselman, R., Dillon, S.R., Madden, K., Xu, W., Parrish-Novak, J., Foster, D., Lofton-Day, C., et al. (2000). TACI and BCMA are receptors for a TNF homologue implicated in B-cell autoimmune disease. *Nature* 404, 995–999. <https://doi.org/10.1038/35010115>.
- Habib, T., Senadheera, S., Weinberg, K., and Kaushansky, K. (2002). The common gamma chain ( $\gamma$ c) is a required signaling component of the IL-21 receptor and supports IL-21-induced cell proliferation via JAK3. *Biochemistry* 41, 8725–8731. <https://doi.org/10.1021/bi0202023>.
- Hawse, W.F., Sheehan, R.P., Miskov-Zivanov, N., Menk, A.V., Kane, L.P., Faeder, J.R., and Morel, P.A. (2015). Cutting edge: differential regulation of PTEN by TCR, akt, and FoxO1 controls CD4+ T cell fate decisions. *J. Immunol.* 194, 4615–4619. <https://doi.org/10.4049/jimmunol.1402554>.
- Herling, M., Patel, K.A., Hsi, E.D., Chang, K.C., Rassidakis, G.Z., Ford, R., and Jones, D. (2007). TCL1 in B-cell tumors retains its normal b-cell pattern of regulation and is a marker of differentiation stage. *Am. J. Surg. Pathol.* 31, 1123–1129. <https://doi.org/10.1097/pas.0b013e31802e2201>.
- Herling, M., Patel, K.A., Weit, N., Lilienthal, N., Hallek, M., Keating, M.J., and Jones, D. (2009). High TCL1 levels are a marker of B-cell receptor pathway responsiveness and adverse outcome in chronic lymphocytic leukemia. *Blood* 114, 4675–4686. <https://doi.org/10.1182/blood-2009-03-208256>.
- Hildebrand, J.M., Luo, Z., Manske, M.K., Price-Troska, T., Ziesmer, S.C., Lin, W., Hostager, B.S., Slager, S.L., Witzig, T.E., Ansell, S.M., et al. (2010). A BAFF-R mutation associated with non-Hodgkin lymphoma alters TRAF recruitment and reveals new insights into BAFF-R signaling. *J. Exp. Med.* 207, 2569–2579. <https://doi.org/10.1084/jem.20100857>.
- Hobeika, E., Levit-Zerdoun, E., Anastasopoulou, V., Pohlmeier, R., Altmeier, S., Alsadeq, A., Dobenecker, M.W., Pelanda, R., and Reth, M. (2015). CD19 and BAFF-R can signal to promote B-cell survival in the absence of Syk. *EMBO J.* 34, 925–939. <https://doi.org/10.15252/embo.201489732>.
- Hoffmann, F.S., Kuhn, P.H., Laurent, S.A., Hauck, S.M., Berer, K., Wendlinger, S.A., Krumbholz, M., Khademi, M., Olsson, T., Dreyling, M., et al. (2015). The immunoregulator soluble TACI is released by ADAM10 and reflects B cell activation in autoimmunity. *J. Immunol.* 194, 542–552. <https://doi.org/10.4049/jimmunol.1402070>.
- Jacobi, A.M., Huang, W., Wang, T., Freimuth, W., Sanz, I., Furie, R., Mackay, M., Aranow, C., Diamond, B., and Davidson, A. (2010). Effect of long-term belimumab treatment on B cells in systemic lupus erythematosus: extension of a phase II, double-blind, placebo-controlled, dose-ranging study. *Arthritis Rheum.* 62, 201–210. <https://doi.org/10.1002/art.27189>.
- Jacque, E., Schweighoffer, E., Tybulewicz, V.L., and Ley, S.C. (2015). BAFF activation of the ERK5 MAP kinase pathway regulates B cell survival. *J. Exp. Med.* 212, 883–892. <https://doi.org/10.1084/jem.20142127>.
- Jellusova, J., Miletic, A.V., Cato, M.H., Lin, W.W., Hu, Y., Bishop, G.A., Shlomchik, M.J., and Rickert, R.C. (2013). Context-specific BAFF-R signaling by the NF- $\kappa$ B and PI3K pathways. *Cell Rep.* 5, 1022–1035. <https://doi.org/10.1016/j.celrep.2013.10.022>.
- Keppeler, S.J., Gasparini, F., Burbage, M., Aggarwal, S., Frederico, B., Geha, R.S., Way, M., Bruckbauer, A., and Batista, F.D. (2015). Wiskott-aldrich syndrome interacting protein deficiency uncovers the role of the Co-receptor CD19 as a generic hub for PI3 kinase signaling in B cells. *Immunity* 43, 660–673. <https://doi.org/10.1016/j.immuni.2015.09.004>.
- Kim, D., Langmead, B., and Salzberg, S.L. (2015). HISAT: a fast spliced aligner with low memory requirements. *Nat. Methods* 12, 357–360. <https://doi.org/10.1038/nmeth.3317>.
- Kimura, S., Naito, H., Segawa, H., Kuroda, J., Yuasa, T., Sato, K., Yokota, A., Kamitsui, Y., Kawata, E., Ashihara, E., et al. (2005). NS-187, a potent and selective dual Bcr-Abl/Lyn tyrosine kinase inhibitor, is a novel agent for imatinib-resistant leukemia. *Blood* 106, 3948–3954. <https://doi.org/10.1182/blood-2005-06-2209>.

- Klasener, K., Maity, P.C., Hobeika, E., Yang, J., and Reth, M. (2014). B cell activation involves nanoscale receptor reorganizations and inside-out signaling by Syk. *Elife* 3, e02069. <https://doi.org/10.7554/elife.02069>.
- Kowalczyk-Quintas, C., Willen, D., Willen, L., Golob, M., Schuepbach-Malpell, S., Peter, B., Eslami, M., Vigolo, M., Broly, H., Samy, E., et al. (2019). No interactions between heparin and atacept, an antagonist of B cell survival cytokines. *Br. J. Pharmacol.* 176, 4019–4033. <https://doi.org/10.1111/bph.14811>.
- Laine, J., Künstle, G., Obata, T., Sha, M., and Noguchi, M. (2000). The proto-oncogene TCL1 is an Akt kinase coactivator. *Mol. Cell* 6, 395–407. [https://doi.org/10.1016/s1097-2765\(00\)00039-3](https://doi.org/10.1016/s1097-2765(00)00039-3).
- Lang, J., Zhang, B., Kelly, M., Peterson, J.N., Barbee, J., Freed, B.M., Di Santo, J.P., Matsuda, J.L., Torres, R.M., and Pelanda, R. (2017). Replacing mouse BAFF with human BAFF does not improve B-cell maturation in hematopoietic humanized mice. *Blood Adv.* 1, 2729–2741. <https://doi.org/10.1182/bloodadvances.2017010090>.
- Lataretu, M., and Hölzer, M. (2020). RNAflow: an effective and simple RNA-seq differential gene expression pipeline using Nextflow. *Genes* 11, 1487. <https://doi.org/10.3390/genes11121487>.
- Lau, A.W.Y., Turner, V.M., Bourne, K., Hermes, J.R., Chan, T.D., and Brink, R. (2020). BAFFR controls early memory B cell responses but is dispensable for germinal center function. *J. Exp. Med.* 218, e20191167. <https://doi.org/10.1084/jem.20191167>.
- Liao, Y., Smyth, G.K., and Shi, W. (2014). featureCounts: an efficient general purpose program for assigning sequence reads to genomic features. *Bioinformatics* 30, 923–930. <https://doi.org/10.1093/bioinformatics/btt656>.
- Lin, W.Y., Gong, Q., Seshasayee, D., Lin, Z., Ou, Q., Ye, S., Suto, E., Shu, J., Pun Lee, W., Lee, C.W.V., et al. (2007). Anti-BR3 antibodies: a new class of B-cell immunotherapy combining cellular depletion and survival blockade. *Blood* 110, 3959–3967. <https://doi.org/10.1182/blood-2007-04-088088>.
- Losi, C.G., Silini, A., Fiorini, C., Soresina, A., Meini, A., Ferrari, S., Notarangelo, L.D., Lougaris, V., and Plebani, A. (2005). Mutational analysis of human BAFF receptor TNFRSF13C (BAFF-R) in patients with common variable immunodeficiency. *J. Clin. Immunol.* 25, 496–502. <https://doi.org/10.1007/s10875-005-5637-2>.
- Lou, Y., Lu, X., and Dang, X. (2012). FOXO1 up-regulates human L-selectin expression through binding to a consensus FOXO1 motif. *Gene Regul. Syst. Biol.* 6. <https://doi.org/10.4137/grsb.s10343>.
- Love, M.I., Huber, W., and Anders, S. (2014). Moderated estimation of fold change and dispersion for RNA-seq data with DESeq2. *Genome Biol.* 15, 550. <https://doi.org/10.1186/s13059-014-0550-8>.
- Mackay, F., and Schneider, P. (2009). Cracking the BAFF code. *Nat. Rev. Immunol.* 9, 491–502. <https://doi.org/10.1038/nri2572>.
- Mackay, F., Woodcock, S.A., Lawton, P., Ambrose, C., Baetscher, M., Schneider, P., Tschopp, J., and Browning, J.L. (1999). Mice transgenic for BAFF develop lymphocytic disorders along with autoimmune manifestations. *J. Exp. Med.* 190, 1697–1710. <https://doi.org/10.1084/jem.190.11.1697>.
- Maehama, T., and Dixon, J.E. (1998). The tumor suppressor, PTEN/MMAC1, dephosphorylates the lipid second messenger, phosphatidylinositol 3, 4, 5-trisphosphate. *J. Biol. Chem.* 273, 13375–13378. <https://doi.org/10.1074/jbc.273.22.13375>.
- Matsuzaki, H., Daitoku, H., Hatta, M., Tanaka, K., and Fukamizu, A. (2003). Insulin-induced phosphorylation of FKHR (Foxo1) targets to proteasomal degradation. *Proc. Natl. Acad. Sci. USA.* 100, 11285–11290. <https://doi.org/10.1073/pnas.1934283100>.
- Mattila, P.K., Feest, C., Depoil, D., Treanor, B., Montaner, B., Otipoby, K.L., Carter, R., Justement, L.B., Bruckbauer, A., and Batista, F.D. (2013). The actin and tetraspanin networks organize receptor nanoclusters to regulate B cell receptor-mediated signaling. *Immunity* 38, 461–474. <https://doi.org/10.1016/j.immuni.2012.11.019>.
- Mecklenbrauker, I., Kalled, S.L., Leitges, M., Mackay, F., and Tarakhovskiy, A. (2004). Regulation of B-cell survival by BAFF-dependent PKCdelta-mediated nuclear signalling. *Nature* 431, 456–461. <https://doi.org/10.1038/nature02955>.
- Metsalu, T., and Vilo, J. (2015). ClustVis: a web tool for visualizing clustering of multivariate data using Principal Component Analysis and heatmap. *Nucleic Acids Res.* 43, W566–W570. <https://doi.org/10.1093/nar/gkv468>.
- Moore, P.A., Belvedere, O., Orr, A., Pieri, K., LaFleur, D.W., Feng, P., Soppet, D., Charters, M., Gentz, R., Parmelee, D., et al. (1999). BLYS: member of the tumor necrosis factor family and B lymphocyte stimulator. *Science* 285, 260–263. <https://doi.org/10.1126/science.285.5425.260>.
- Müller-Winkler, J., Mitter, R., Rappe, J.C.F., Vanes, L., Schweighoffer, E., Mohammadi, H., Wack, A., and Tybulewicz, V.L.J. (2021). Critical requirement for BCR, BAFF, and BAFFR in memory B cell survival. *J. Exp. Med.* 218, e20191393. <https://doi.org/10.1084/jem.20191393>.
- Nardelli, B., Belvedere, O., Roschke, V., Moore, P.A., Olsen, H.S., Migone, T.S., Sosnovtseva, S., Carrell, J.A., Feng, P., Giri, J.G., and Hilbert, D.M. (2001). Synthesis and release of B-lymphocyte stimulator from myeloid cells. *Blood* 97, 198–204. <https://doi.org/10.1182/blood.v97.1.198>.
- Ntellas, P., Dardiotis, E., Sevdali, E., Siokas, V., Aloizou, A.M., Tsimtsi, G., Geremenis, A.E., Hadjigeorgiou, G.M., Eibel, H., and Speletas, M. (2020). TNFRSF13C/BAFFR P21R and H159Y polymorphisms in multiple sclerosis. *Mult. Scler. Relat. Disord.* 37, 101422. <https://doi.org/10.1016/j.msard.2019.101422>.
- O'Connor, B.P., Raman, V.S., Erickson, L.D., Cook, W.J., Weaver, L.K., Ahonen, C., Lin, L.L., Mantchev, G.T., Bram, R.J., and Noelle, R.J. (2004). BCMA is essential for the survival of long-lived bone marrow plasma cells. *J. Exp. Med.* 199, 91–98. <https://doi.org/10.1084/jem.20031330>.
- Otipoby, K.L., Sasaki, Y., Schmidt-Suppran, M., Patke, A., Gareus, R., Pasparakis, M., Tarakhovskiy, A., and Rajewsky, K. (2008). BAFF activates Akt and Erk through BAFF-R in an IKK1-dependent manner in primary mouse B cells. *Proc. Natl. Acad. Sci. USA.* 105, 12435–12438. <https://doi.org/10.1073/pnas.0805460105>.
- Park, M.K., Yao, Y., Xia, W., Setijono, S.R., Kim, J.H., Vila, I.K., Chiu, H.H., Wu, Y., Billalabeitia, E.G., Lee, M.G., et al. (2019). PTEN self-regulates through USP11 via the PI3K-FOXO pathway to stabilize tumor suppression. *Nat. Commun.* 10, 636. <https://doi.org/10.1038/s41467-019-08481-x>.
- Patke, A., Mecklenbrauker, I., Erdjument-Bromage, H., Tempst, P., and Tarakhovskiy, A. (2006). BAFF controls B cell metabolic fitness through a PKC beta- and Akt-dependent mechanism. *J. Exp. Med.* 203, 2551–2562. <https://doi.org/10.1084/jem.20060990>.
- Pekarsky, Y., Koval, A., Hallas, C., Bichi, R., Tresini, M., Malstrom, S., Russo, G., Tschlis, P., and Croce, C.M. (2000). Tcl1 enhances Akt kinase activity and mediates its nuclear translocation. *Proc. Natl. Acad. Sci. USA.* 97, 3028–3033. <https://doi.org/10.1073/pnas.97.7.3028>.
- Pekarsky, Y., Palamarchuk, A., Maximov, V., Efanov, A., Nazaryan, N., Santanam, U., Rassenti, L., Kipps, T., and Croce, C.M. (2008). Tcl1 functions as a transcriptional regulator and is directly involved in the pathogenesis of CLL. *Proc. Natl. Acad. Sci. USA.* 105, 19643–19648. <https://doi.org/10.1073/pnas.0810965105>.
- Peter, A.S., Roth, E., Schulz, S.R., Fraedrich, K., Steinmetz, T., Damm, D., Hauke, M., Richel, E., Mueller-Schmucker, S., Habenicht, K., et al. (2021). A pair of noncompeting neutralizing human monoclonal antibodies protecting from disease in a SARS-CoV-2 infection model. *Eur. J. Immunol.* 770–783. <https://doi.org/10.1002/eji.202149374>.
- Pieper, K., Rizzi, M., Speletas, M., Smulski, C.R., Sic, H., Kraus, H., Salzer, U., Fiala, G.J., Schamel, W.W., Lougaris, V., et al. (2014). A common single nucleotide polymorphism impairs B-cell activating factor receptor's multimerization, contributing to common variable immunodeficiency. *J. Allergy Clin. Immunol.* 133, 1222–1225.e10. <https://doi.org/10.1016/j.jaci.2013.11.021>.
- Puga, I., Cols, M., Barra, C.M., He, B., Cassis, L., Gentile, M., Comerma, L., Chorny, A., Shan, M., Xu, W., et al. (2011). B cell-helper neutrophils stimulate the diversification and production of immunoglobulin in the marginal zone of the spleen. *Nat. Immunol.* 13, 170–180. <https://doi.org/10.1038/ni.2194>.
- Rasband, W.S. (1997–2018). Image J (U. S. National Institutes of Health).
- Reth, M. (1992). Antigen receptors on B lymphocytes. *Annu. Rev. Immunol.* 10, 97–121. <https://doi.org/10.1146/annurev.iy.10.040192.000525>.

- Rolli, V., Gallwitz, M., Wossning, T., Flemming, A., Schamel, W.W., Zürn, C., and Reth, M. (2002). Amplification of B cell antigen receptor signaling by a Syk/ITAM positive feedback loop. *Mol. Cell* 10, 1057–1069. [https://doi.org/10.1016/s1097-2765\(02\)00739-6](https://doi.org/10.1016/s1097-2765(02)00739-6).
- Sander, S., Chu, V.T., Yasuda, T., Franklin, A., Graf, R., Calado, D.P., Li, S., Imami, K., Selbach, M., Di Virgilio, M., et al. (2015). PI3 kinase and FOXO1 transcription factor Activity differentially control B cells in the germinal center light and dark zones. *Immunity* 43, 1075–1086. <https://doi.org/10.1016/j.immuni.2015.10.021>.
- Sasaki, Y., Casola, S., Kutok, J.L., Rajewsky, K., and Schmidt-Supprian, M. (2004). TNF family member B cell-activating factor (BAFF) receptor-dependent and -independent roles for BAFF in B cell physiology. *J. Immunol.* 173, 2245–2252. <https://doi.org/10.4049/jimmunol.173.4.2245>.
- Schiemann, B., Gommerman, J.L., Vora, K., Cachero, T.G., Shulga-Morskaya, S., Dobles, M., Frew, E., and Scott, M.L. (2001). An essential role for BAFF in the normal development of B cells through a BCMA-independent pathway. *Science* 293, 2111–2114. <https://doi.org/10.1126/science.1061964>.
- Schneider, P., Willen, L., and Smulski, C.R. (2014). Tools and techniques to study ligand-receptor interactions and receptor activation by TNF superfamily members. *Methods Enzymol.* 545, 103–125. <https://doi.org/10.1016/B978-0-12-801430-1.00005-6>.
- Schweighoffer, E., and Tybulewicz, V.L. (2018). Signalling for B cell survival. *Curr. Opin. Cell Biol.* 51, 8–14. <https://doi.org/10.1016/j.ceb.2017.10.002>.
- Schweighoffer, E., Vanes, L., Nys, J., Cantrell, D., McCleary, S., Smithers, N., and Tybulewicz, V.L. (2013). The BAFF receptor transduces survival signals by co-opting the B cell receptor signaling pathway. *Immunity* 38, 475–488. <https://doi.org/10.1016/j.immuni.2012.11.015>.
- Shiow, L.R., Rosen, D.B., Brdicková, N., Xu, Y., An, J., Lanier, L.L., Cyster, J.G., and Matloubian, M. (2006). CD69 acts downstream of interferon- $\alpha/\beta$  to inhibit S1P1 and lymphocyte egress from lymphoid organs. *Nature* 440, 540–544. <https://doi.org/10.1038/nature04606>.
- Sic, H., Kraus, H., Madl, J., Flittner, K.A., von Münchow, A.L., Pieper, K., Rizzi, M., Kienzler, A.K., Ayata, K., Rauer, S., et al. (2014). Sphingosine-1-phosphate receptors control B-cell migration through signaling components associated with primary immunodeficiencies, chronic lymphocytic leukemia, and multiple sclerosis. *J. Allergy Clin. Immunol.* 134, 420–428.e15. <https://doi.org/10.1016/j.jaci.2014.01.037>.
- Sic, H., Speletas, M., Cornacchione, V., Seidl, M., Beibel, M., Linghu, B., Yang, F., Sevdali, E., Germeis, A.E., Oakeley, E.J., et al. (2017). An activating janus kinase-3 mutation is associated with cytotoxic T lymphocyte antigen-4-dependent immune dysregulation syndrome. *Front. Immunol.* 8, 1824. <https://doi.org/10.3389/fimmu.2017.01824>.
- Smith, S.H., and Cancro, M.P. (2003). Cutting edge: B cell receptor signals regulate BLyS receptor levels in mature B cells and their immediate progenitors. *J. Immunol.* 170, 5820–5823. <https://doi.org/10.4049/jimmunol.170.12.5820>.
- Smulski, C.R., Kury, P., Seidel, L.M., Staiger, H.S., Edinger, A.K., Willen, L., Seidl, M., Hess, H., Salzer, U., Rolink, A.G., et al. (2017). BAFF- and TACI-dependent processing of BAFFR by ADAM proteases regulates the survival of B cells. *Cell Rep.* 18, 2189–2202. <https://doi.org/10.1016/j.celrep.2017.02.005>.
- Smulski, C.R., Zhang, L., Burek, M., Teixidó Rubio, A., Briem, J.S., Sica, M.P., Sevdali, E., Vigolo, M., Willen, L., Odermatt, P., et al. (2022). Ligand-independent oligomerization of TACI is controlled by the transmembrane domain and regulates proliferation of activated B cells. *Cell Rep.* 38, 110583. <https://doi.org/10.1016/j.celrep.2022.110583>.
- Song, M.S., Salmena, L., and Pandolfi, P.P. (2012). The functions and regulation of the PTEN tumour suppressor. *Nat. Rev. Mol. Cell Biol.* 13, 283–296. <https://doi.org/10.1038/nrm3330>.
- Stambolic, V., Suzuki, A., de la Pompa, J.L., Brothers, G.M., Mirtsos, C., Sasaki, T., Ruland, J., Penninger, J.M., Siderovski, D.P., and Mak, T.W. (1998). Negative regulation of PKB/Akt-dependent cell survival by the tumor suppressor PTEN. *Cell* 95, 29–39. [https://doi.org/10.1016/s0092-8674\(00\)81780-8](https://doi.org/10.1016/s0092-8674(00)81780-8).
- Steri, M., Orrù, V., Idda, M.L., Pitzalis, M., Pala, M., Zara, I., Sidore, C., Faà, V., Floris, M., Deiana, M., et al. (2017). Overexpression of the cytokine BAFF and autoimmunity risk. *N. Engl. J. Med.* 376, 1615–1626. <https://doi.org/10.1056/nejmoa1610528>.
- Stohl, W., Hiepe, F., Latinis, K.M., Thomas, M., Scheinberg, M.A., Clarke, A., Aranow, C., Wellborne, F.R., Abud-Mendoza, C., Hough, D.R., et al. (2012). Belimumab reduces autoantibodies, normalizes low complement levels, and reduces select B cell populations in patients with systemic lupus erythematosus. *Arthritis Rheum.* 64, 2328–2337. <https://doi.org/10.1002/art.34400>.
- Szklarczyk, D., Gable, A.L., Nastou, K.C., Lyon, D., Kirsch, R., Pyysalo, S., Doncheva, N.T., Legeay, M., Fang, T., Bork, P., et al. (2020). The STRING database in 2021: customizable protein–protein networks, and functional characterization of user-uploaded gene/measurement sets. *Nucleic Acids Res.* 49, D605–D612. <https://doi.org/10.1093/nar/gkaa1074>.
- Tak, P.P., Thurlings, R.M., Rossier, C., Nestorov, I., Dimic, A., Mircetic, V., Rischmueller, M., Nasonov, E., Shmidt, E., Emery, P., and Munafo, A. (2008). Atacept in patients with rheumatoid arthritis: results of a multicenter, phase Ib, double-blind, placebo-controlled, dose-escalating, single- and repeated-dose study. *Arthritis Rheum.* 58, 61–72. <https://doi.org/10.1002/art.23178>.
- Thien, M., Phan, T.G., Gardam, S., Amesbury, M., Basten, A., Mackay, F., and Brink, R. (2004). Excess BAFF rescues self-reactive B cells from peripheral deletion and allows them to enter forbidden follicular and marginal zone niches. *Immunity* 20, 785–798. <https://doi.org/10.1016/j.immuni.2004.05.010>.
- van Vollenhoven, R.F., Kinnman, N., Vincent, E., Wax, S., and Bathon, J. (2011). Atacept in patients with rheumatoid arthritis and an inadequate response to methotrexate: results of a phase II, randomized, placebo-controlled trial. *Arthritis Rheum.* 63, 1782–1792. <https://doi.org/10.1002/art.30372>.
- Vigolo, M., Chambers, M.G., Willen, L., Chevalley, D., Maskos, K., Lammens, A., Tardivel, A., Das, D., Kowalczyk-Quintas, C., Schuepbach-Mallepell, S., et al. (2018). A loop region of BAFF controls B cell survival and regulates recognition by different inhibitors. *Nat. Commun.* 9, 1199. <https://doi.org/10.1038/s41467-018-03323-8>.
- Vugmeyster, Y., Seshasayee, D., Chang, W., Storn, A., Howell, K., Sa, S., Nelson, T., Martin, F., Grewal, I., Gilkerson, E., et al. (2006). A soluble BAFF antagonist, BR3-Fc, decreases peripheral blood B cells and lymphoid tissue marginal zone and follicular B cells in cynomolgus monkeys. *Am. J. Pathol.* 168, 476–489. <https://doi.org/10.2353/ajpath.2006.050600>.
- Warnatz, K., Salzer, U., Rizzi, M., Fischer, B., Gutenberger, S., Böhm, J., Kienzler, A.K., Pan-Hammarström, Q., Hammarström, L., Rakhmanov, M., et al. (2009). B-cell activating factor receptor deficiency is associated with an adult-onset antibody deficiency syndrome in humans. *Proc. Natl. Acad. Sci. USA.* 106, 13945–13950. <https://doi.org/10.1073/pnas.0903543106>.
- Willmann, K.L., Klaver, S., Doğu, F., Santos-Valente, E., Garnarcz, W., Bilic, I., Mace, E., Salzer, U., Domínguez Conde, C., Sic, H., et al. (2014). Biallelic loss-of-function mutation in NIK causes a primary immunodeficiency with multifaceted aberrant lymphoid immunity. *Nat. Commun.* 5, 5360. <https://doi.org/10.1038/ncomms6360>.
- Woodland, R.T., Fox, C.J., Schmidt, M.R., Hammerman, P.S., Opferman, J.T., Korsmeyer, S.J., Hilbert, D.M., and Thompson, C.B. (2008). Multiple signaling pathways promote B lymphocyte stimulator dependent B-cell growth and survival. *Blood* 111, 750–760. <https://doi.org/10.1182/blood-2007-03-077222>.
- Yang, J., and Reth, M. (2010). The dissociation activation model of B cell antigen receptor triggering. *FEBS Lett.* 584, 4872–4877. <https://doi.org/10.1016/j.febslet.2010.09.045>.
- Yeh, T.W., Okano, T., Naruto, T., Yamashita, M., Okamura, M., Tanita, K., Du, L., Pan-Hammarström, Q., Mitsuiki, N., Okada, S., et al. (2020).

APRIL-dependent lifelong plasmacyte maintenance and immunoglobulin production in humans. *J. Allergy Clin. Immunol.* *146*, 1109–1120.e4. <https://doi.org/10.1016/j.jaci.2020.03.025>.

Yu, X., Tsibane, T., McGraw, P.A., House, F.S., Keefer, C.J., Hicar, M.D., Tumphey, T.M., Pappas, C., Perrone, L.A., Martinez, O., et al. (2008). Neutralizing

antibodies derived from the B cells of 1918 influenza pandemic survivors. *Nature* *455*, 532–536. <https://doi.org/10.1038/nature07231>.

Yusuf, I., Zhu, X., Kharas, M.G., Chen, J., and Fruman, D.A. (2004). Optimal B-cell proliferation requires phosphoinositide 3-kinase-dependent inactivation of FOXO transcription factors. *Blood* *104*, 784–787. <https://doi.org/10.1182/blood-2003-09-3071>.

STAR★METHODS

KEY RESOURCES TABLE

REAGENT OR RESOURCE	SOURCE	IDENTIFIER
<b>Antibodies</b>		
Rabbit anti-CD79A	Cell Signaling Technology	Cat# 3351; RRID: AB_2075745
Rabbit anti-phospho-CD79A (Tyr182)	Cell Signaling Technology	Cat# 5173T; RRID: AB_10694763
Rabbit anti-CD79B (clone D7V2F)	Cell Signaling Technology	Cat# 96024; RRID: AB_2800254
Mouse anti-AKT (clone 40D4)	Cell Signaling Technology	Cat# 2920; RRID: AB_1147620
Rabbit anti-phospho-AKT (Ser473; clone D9E)	Cell Signaling Technology	Cat# 4060; RRID: AB_2315049
Rabbit anti-CD19	Cell Signaling Technology	Cat# 3574; RRID: AB_2275523
Rabbit anti-phospho-CD19 (Tyr531)	Cell Signaling Technology	Cat# 3571; RRID: AB_2072836
Rabbit anti-PTEN (clone D4.3)	Cell Signaling Technology	Cat# 9188; RRID: AB_2253290
Rabbit anti-4E-BP1	Cell Signaling Technology	Cat# 9452; RRID: AB_331692
Rabbit anti-phospho-4E-BP1 (Ser65; clone 174A9)	Cell Signaling Technology	Cat# 9456; RRID: AB_823413
Rabbit anti-phospho-SYK (Tyr525/526; clone C87C1)	Cell Signaling Technology	Cat# 2710; RRID: AB_2197222
Rabbit anti-phospho-S6 Ribosomal Protein (Ser240/244; clone D68F8)	Cell Signaling Technology	Cat# 5364; RRID: AB_10694233
Mouse anti-FoxO1 (clone D7C1H)	Cell Signaling Technology	Cat# 14952; RRID: AB_10694233
Rabbit anti-MCL-1 (clone D35A5)	Cell Signaling Technology	Cat# 5453; RRID: AB_10694494
Rabbit anti-BCL-xL (clone 54H6)	Cell Signaling Technology	Cat# 2764; RRID: AB_2228008
Rabbit anti-TRAF3 (clone D1N5B)	Cell Signaling Technology	Cat# 61095S; RRID: AB_2799601
Rabbit anti-phospho-Src family [Tyr416; corresponds to Tyr419 of human Src; clone D49G4]	Cell Signaling Technology	Cat# 6943; RRID: AB_10013641
Rabbit anti-phospho-LYN (Tyr507)	Cell Signaling Technology	Cat# 2731; RRID: AB_2138262
Rabbit anti-LYN (clone C13F9)	Cell Signaling Technology	Cat# 2796; RRID: AB_2138391
Rabbit anti-STAT5 (clone 3H7)	Cell Signaling Technology	Cat# 9358; RRID: AB_659905
Rabbit anti-phospho-FOXO1 (Ser256)	Sigma-Aldrich	Cat# SAB4300094; RRID: AB_10626763
Rabbit anti-NFκB p52	Millipore	Cat# 05-361; RRID: AB_309692
Mouse anti-β-actin (clone AC15)	Sigma Aldrich	Cat# A5441; RRID: AB_476744
Rabbit anti-BAFFR-CT	Enzo Biochem	Cat# ADI-905-305; RRID: AB_10618752
Mouse anti-BAFFR (clone H1)	Santa Cruz	Cat# sc-365410; RRID: AB_10842301
Goat F(ab') <sub>2</sub> anti-IgM	SouthernBiotech	Cat# 2022-01; RRID: AB_2795610
Goat F(ab') <sub>2</sub> anti-IgA+IgG+IgM (H+L)	Jackson ImmunoResearch Laboratories	Cat# 109-006-064; RRID: AB_2337548
Goat F(ab') <sub>2</sub> anti-IgD	SouthernBiotech	Cat# 2032-01; RRID: AB_2795634
Peroxidase AffiniPure donkey anti-mouse IgG (H+L)	Jackson ImmunoResearch Laboratories	Cat# 715-035-150; RRID: AB_2340770
Peroxidase AffiniPure donkey anti-rabbit IgG (H+L)	Jackson ImmunoResearch Laboratories	Cat# 711-035-152; RRID: AB_10015282
Peroxidase AffiniPure donkey anti-goat IgG (H+L)	Jackson ImmunoResearch Laboratories	Cat# 705-035-003; RRID: AB_2340390
Mouse anti-CD19 APC/Cy7 (clone <a href="#">HIB19</a> )	Biolegend	Cat# 302218; RRID: AB_314248
Mouse anti-CD19 Pe/Cy7 (clone <a href="#">SJ25C1</a> )	BD Biosciences	Cat# 557835; RRID: AB_396893
Mouse anti-BAFFR PE (clone 11C1)	Biolegend	Cat# 316906; RRID: AB_528983
Mouse anti-BAFFR Alexa Fluor 647 (clone 11C1)	Biolegend	Cat# 316914; RRID: AB_2203680
Rat anti-TACI APC (clone 1A1)	Biolegend	Cat# 311912; RRID: AB_2565423
Goat F(ab') <sub>2</sub> anti-IgD FITC	SouthernBiotech	Cat# 2032-02; RRID: AB_2687521
Goat F(ab') <sub>2</sub> anti-IgD (PE)	SouthernBiotech	Cat# 2032-09; RRID: AB_2795636

(Continued on next page)

**Continued**

REAGENT OR RESOURCE	SOURCE	IDENTIFIER
Mouse anti-IgD PerCP/Cy5.5 (clone IA6-2)	Biolegend	Cat# 348,208; RRID: AB_10641706
Mouse anti-IgM APC/Cy7 (clone MHM-88)	Biolegend	Cat# 314520; RRID: AB_10900422
Donkey F(ab') <sub>2</sub> anti-human IgM Cy5	Jackson ImmunoResearch	Cat# 709-176-073; RRID: AB_2340579
Goat F(ab') <sub>2</sub> anti-human IgA Alexa Fluor 647	Jackson ImmunoResearch	Cat# 109-496-011; RRID: AB_2337895
Goat F(ab') <sub>2</sub> anti-human IgA FITC	SouthernBiotech	Cat# 2052-02; RRID: AB_2795710
Goat F(ab') <sub>2</sub> anti-human IgG Alexa Fluor 647	Jackson ImmunoResearch	Cat# 109-496-098; RRID: AB_2337899
Rat anti-human IgG Fc PE (clone M1310G05)	Biolegend	Cat# 410708; RRID: AB_2565786
Mouse anti-human CD79A Alexa Fluor 488 (Clone 706931)	R&D systems	Cat# FAB69201G; RRID: N/A
Mouse anti-human CD79B PE (CB3-1)	Biolegend	Cat# 341404; RRID: AB_1595454
Mouse anti-human CD79B APC (CB3-1)	Biolegend	Cat# 341406; RRID: AB_1626190
Mouse anti-human CD27 PE (clone M-T271)	Biolegend	Cat# 356406; RRID: AB_2561825
Mouse anti-human CD27 PerCP/Cy5.5 (clone M-T271)	Biolegend	Cat# 356408; RRID: AB_2561906
Mouse anti-human CD27 PE/Cy7 (clone M-T271)	Biolegend	Cat# 356412; RRID: AB_2562258
Mouse anti-human CD27 Brilliant Violet 421 (clone M-T271)	Biolegend	Cat# 356418; RRID: AB_2562599
Mouse anti-human CXCR4 Brilliant Violet 421 (clone 12G5)	Biolegend	Cat# 306518; RRID: AB_11146018
Mouse anti-human CD54 Alexa Fluor 647 (clone HCD54)	Biolegend	Cat# 322718; RRID: AB_2248731
Mouse anti-human CD62L APC (clone DREG-56)	Biolegend	Cat# 304810; RRID: AB_314470
Mouse anti-human CD69 PE (clone FN50)	Biolegend	Cat# 310906; RRID: AB_314841
Mouse anti-human CD83 Pe/Cy5 (clone HB15e)	Biolegend	Cat# 305310; RRID: AB_314518
Mouse anti-human CD98 FITC (clone MEM-108)	Biolegend	Cat# 315603; RRID: AB_2190795
Mouse anti-human IL21R PE (clone 2G1-K12)	Biolegend	Cat# 347806; RRID: AB_2123990
Mouse anti-human GARP (LRRC32) Brilliant Violet 421 (clone 7B11)	Biolegend	Cat# 352509; RRID: AB_2562249
Mouse anti-human CD172a/b (SIRPα/β) FITC (clone SE5A5)	Biolegend	Cat# 323820; RRID: AB_2749933
Mouse anti-human Ig light chain kappa FITC (clone MHK-49)	Biolegend	Cat# 316506; RRID: AB_493611
Mouse anti-human Ig light chain lambda PE (clone MHL-38)	Biolegend	Cat# 316607; RRID: AB_493626
Mouse anti-human IgD PerCP/Cy5.5 (clone IA6-2)	Biolegend	Cat# 348208; RRID: AB_10641706
Rabbit anti-human phospho-S6 (S240/S244) PE (clone D68F8)	Cell Signaling Technology	Cat# 14236S; RRID: AB_2798433
Mouse anti-human BCL-2 PE (clone 100)	Biolegend	Cat# 658708; RRID: AB_2563282
Rat anti-human IRF4 Pe/Cy7 (clone IRF4.3E4)	Biolegend	Cat# 646413; RRID: AB_2728479
Recombinant anti-human/mouse PTEN APC (clone REA270)	Miltenyi Biotec	Cat# 130-103-716; RRID: AB_2653287
Mouse anti-human CD79A PE (clone HM47)	Beckman Coulter	Cat# IM2221; RRID: AB_131316
Mouse anti-human CD79A Alexa Fluor 647 (clone HM47)	Biolegend	Cat# 333515; RRID: AB_2734330
Rat anti-human IL-10 Alexa Fluor 488 (clone JES3-9D7)	Biolegend	Cat# 501413; RRID: AB_493317
Mouse anti-human IL-1β Alexa Fluor 647 (clone JK1B-1)	Biolegend	Cat# 508207; RRID: AB_604133
Rat anti-human IL-6 PerCP/Cy5.5 (clone MQ2-13A5)	Biolegend	Cat# 501117; RRID: AB_2572039
Mouse anti-human TCL1A (clone eBio1-21 (1-21))	eBioscience	Cat# 17-6699-42; RRID: AB_11149309
Mouse anti-human CD27 biotinylated	Biolegend	Cat# 356426; RRID: AB_2571912
Goat F(ab') <sub>2</sub> Anti-Human IgA biotinylated	SouthernBiotech	Cat# 2052-08; RRID: AB_2687520
Rat Anti-Human IgG Fc biotinylated	Biolegend	Cat# 410718; RRID: AB_2721499
Goat F(ab') <sub>2</sub> Anti-Human IgM biotinylated	SouthernBiotech	Cat# 2022-08; RRID: AB_2795613
Goat F(ab') <sub>2</sub> Anti-Human IgD biotinylated	SouthernBiotech	Cat# 2032-08; RRID: AB_2795635
Mouse anti-His Tag Alexa Fluor 647 (clone J095G46)	Biolegend	Cat# 362611; RRID: AB_2721401
Donkey F(ab') <sub>2</sub> anti-rabbit IgG (H+L) Alexa Fluor 647	Jackson ImmunoResearch	Cat# 711-606-152; RRID: AB_2340625

(Continued on next page)

REAGENT OR RESOURCE	SOURCE	IDENTIFIER
<b>Continued</b>		
<b>Chemicals, peptides, and recombinant proteins</b>		
BAFF	<a href="#">Smulski et al., 2017</a>	N/A
CD40L	<a href="#">Smulski et al., 2017</a>	N/A
SARS-Cov2 spike protein	ThermoFisher	Cat# RP-87680
SYK inhibitor (R406)	Selleckchem	Cat# S2194; CAS 841290-81-1
Dual BCR-ABL/LYN inhibitor (Bafetinib/INNO-406)	Selleckchem	Cat# S1369; CAS 859212-16-1
PI3K $\delta$ inhibitor (nemoralisib/GSK2269557)	Selleckchem	Cat# S7937; CAS 1254036-71-9
PKD1 inhibitor (BX-795)	Selleckchem	Cat# S1274; CAS 702675-74-9
FOXO1 inhibitor (AS1842856)	Selleckchem	Cat# S8222; CAS 836620-48-5
NIK inhibitor (SMI1)	Hycultec	Cat# HY112433; CAS 1660114-31-7
human monoclonal IgG1 $\lambda$ anti-BAFF antibody belimumab (Benlysta)	GlaxoSmithKline Pharmaceuticals	CAS 356547-88-1
hTACI (aa 31–110)-hIgG1 Fc (aa 245–470)	<a href="#">Kowalczyk-Quintas et al., 2019</a>	N/A
Fixable viability dye eFluor450	eBioscience	Cat# 65-0863-14
Brefeldin A	Biolegend	Cat# 420601
<b>Critical commercial assays</b>		
Neon Transfection System 10 $\mu$ L Kit	Thermo Fischer Scientific	Cat# MPK1096
NEBuilder HiFi DNA Assembly Cloning Kit	New England Biolabs	Cat# E5520S
jetPEI	Polyplus transfection	Cat# 101-10N
<b>Experimental models: Cell lines</b>		
DG-75	DSMZ	Cat# ACC 83
HEK 293T	DSMZ	Cat# ACC 635
<b>Oligonucleotides</b>		
5'-TCCTCCATGGCAACTACACGTGG-3'	Integrated DNA Technologies	Hs.Cas9.CD79A.1.AB
5'-AACACCTCGGAGGTCTACCAGGG-3'	Integrated DNA Technologies	Hs.Cas9.CD79B.1.AA
5'-CCTTCCAAGGACGTCATGCAGGGC-3'	Integrated DNA Technologies	N/A
5'-TTAATAACATCACCATGCACAGG-3'	Integrated DNA Technologies	Hs.Cas9.LYN.1.AE
5'-CTCACCGTCCTGTCTCCGTCGG-3'	Integrated DNA Technologies	N/A
5'-GTTTGAAGAGGATCACACTCGG-3'	Integrated DNA Technologies	Hs.Cas9.CD27.1.AF
5'-CAAATACACGAAGTCTCTCCC-3'	Integrated DNA Technologies	Hs.Cas9.TCL1A.1.AE
5'-CTCGGGAAGGTACCAAGGAT-3'	Integrated DNA Technologies	Hs.Cas9.TNFRSF13B.1.AA
<b>Software and algorithms</b>		
Flow Jo_v10	Flow Jo	<a href="https://www.flowjo.com/solutions/flowjo">https://www.flowjo.com/solutions/flowjo</a> RRID: SCR_008520
GraphPad Prism 8.4	GraphPad	<a href="https://www.graphpad.com/scientific-software/prism">https://www.graphpad.com/scientific-software/prism</a> RRID: SCR_002798
Image J V.2.3.0	<a href="#">Rasband, 1997-2018</a>	<a href="http://imagej.net/ImageJ">http://imagej.net/ImageJ</a> RRID: SCR_003070
ClustVis	<a href="#">Metsalu and Vilo, 2015</a>	<a href="https://biit.cs.ut.ee/clustvis/">https://biit.cs.ut.ee/clustvis/</a> ; RRID: SCR_017133
String	<a href="#">Szklarczyk et al., 2020</a>	<a href="https://www.string-db.org/">https://www.string-db.org/</a> ; RRID: SCR_005223

## RESOURCE AVAILABILITY

### Lead contact

Further information and requests for resources and reagents should be directed to and will be fulfilled by the lead contact, Hermann Eibel ([hermann.eibel@uniklinik-freiburg.de](mailto:hermann.eibel@uniklinik-freiburg.de)).

### Materials availability

Plasmids generated in this study are submitted to Addgene.

### Data and code availability

Code and data for the RNA-Seq analysis is available at <https://www.rna.uni-jena.de/supplements/baffr/> and <https://osf.io/2jyud/>. This paper does not report original code.

Any additional information required to reanalyze the data reported in this paper is available from the [lead contact](#) upon request.

## EXPERIMENTAL MODEL AND SUBJECT DETAILS

### Primary cells and cell lines

Human PBMCs, HEK293T cells and the EBV-negative Burkitt lymphoma cell line DG-75 were maintained at 37°C in a 6.5% CO<sub>2</sub> atmosphere in Iscove's medium (Gibco) containing L-glutamine and HEPES, supplemented with 10% heat-inactivated fetal calf serum (FCS) and 100 U/mL penicillin/streptomycin. All experiments involving human samples were carried out in accordance with the ethics approvals 169/13 and 428/17 including all amendments to HE issued by the Ethics Commission of the Albert-Ludwigs-University of Freiburg.

## METHOD DETAILS

### Plasmids, transfection and transduction

The coding sequences of *TNFRSF13C*, *CD79A*, *CD79B* genes were synthesized *in vitro* (IDT-DNA) and cloned into the pNL-CEF-eCFP, pNL-CEF-eYFP or pNL-CEF-RFP lentiviral expression vectors (Sic et al., 2014) with the NEBuilder HiFi DNA Assembly kit. For the generation of the IgA1 and IgG1 BCRs, the bicistronic pNL-CEF-IRES-eGFP lentiviral expression vector has been used as a backbone (Sic et al., 2017). Briefly, the coding sequences of IGHV, IGHA1, IGKV and IGKC were synthesized as one single gBlock gene fragment (IDT-DNA) and inserted upstream of the IRES sequence in the pNL-CEF-IRES-eGFP vector, by replacing a 46 bp fragment; a DNA sequence encoding for a *Thosea asigna* virus 2A (T2A) self-cleaving peptide was included between the IGHA1 and IGKV to separate H- and L-chains after translation. The IgG1 and IgM version were made by replacing the C $\alpha$ 1 coding region of pNL-CEF-IgA1-IRES-eGFP with the C $\gamma$ 1 or C $\mu$  coding regions respectively. The coding sequence of eGFP has been removed from both the pNL-CEF-IgA1-IRES-eGFP and pNL-CEF-IgG1-IRES-eGFP vectors for the generation of cell lines used in FRET experiments. The human constant kappa light (Ensembl: ENSG00000211592), IgA1 (Ensembl: ENSG00000211895), IgG1 (Ensembl: ENSG00000211896) and IgM (Ensembl: ENSG00000211899) heavy chain sequences were derived from the Ensembl genetic sequence database. The monoclonal antibody recognizing the spike Wuhan variant of the SARS-CoV-2 virus is described in Peter et al. (Peter et al., 2021). All constructs were verified by DNA sequencing. Lentiviral particles were produced in HEK293T cells transfected with the different pNL-CEF constructs for BAFFR, CD79A, CD79B, IgA1, IgG1 and IgM together with the packaging plasmid (pCD/NLBH\*) and the envelope plasmid (pVSV-G), with the aid of the JetPEI reagent (Polyplus-transfection) as described before (Sic et al., 2014, 2017). Two days after transfection, virus-containing supernatants were centrifuged, filtered through a 0.2  $\mu$ m syringe filter and centrifuged at 4500 rpm, 4°C, overnight. The next day, the supernatant was discarded and the concentrated virus was used to infect DG-75 wild type,  $\mu$ -heavy chain ( $\mu$ -HC) knockout (KO), BAFFR KO or  $\mu$ -HC KO/BAFFR KO cells, according to the assay. As inactivation of the  $\mu$ -HC locus resulted in the appearance of a cell subset which expressed IgD, these cells were sorted for the generation of IgD<sup>+</sup> DG-75 cell line, while in the case of the spike-specific IgM, IgA or IgG cell lines, only the single BCR-expressing cells (IgD<sup>-</sup>) were sorted.

### Isolation of B cells

PBMCs were isolated from fresh leukoreduction system chambers from healthy donors by Ficoll density gradient centrifugation. Total B cells were purified by immunomagnetic negative selection, using the Human Pan-B cell isolation kit (Biolegend) with a MojoSort magnet (B cell purity  $\geq$  95%). A second isolation step was performed for the purification of naive and switched memory B cells, using biotinylated anti-human CD27 and F(ab')<sub>2</sub> anti-human IgA antibodies for the naive B cells, or F(ab')<sub>2</sub> anti-human IgM and F(ab')<sub>2</sub> anti-human IgD antibodies for the switched memory B cells, followed by magnetic bead-depletion of labeled cells.

### **In vitro activation and inhibition of cells**

Cells were rested at 37°C, 6.5% CO<sub>2</sub> for 1 h prior to any treatment, seeded at 1 million/mL density, and stimulated with BAFF (20 ng/mL for primary cells, 100 ng/mL for cell lines), F(ab')<sub>2</sub> goat anti-human IgM (μ specific; 2 μg/mL), F(ab')<sub>2</sub> goat anti-human IgD (2 μg/mL), F(ab')<sub>2</sub> goat anti-human IgA-IgG-IgM (2 μg/mL), SARS-Cov-2 spike protein (his-tag; 1 μg/mL), CD40L or IL-21. BAFF, CD40L, and IL-21 were produced in house as described (Bossen et al., 2008; Pieper et al., 2014; Schneider et al., 2014; War-natz et al., 2009). CD40L was produced in 293T cells and secreted as multimer into the supernatant. Optimal concentrations were determined before by titrating the proliferation-inducing activity of CD40L supernatants.

The SYK inhibitor R406, the dual BCR-ABL/LYN inhibitor Bafetinib/INNO-406, the PI3K inhibitor nemralisib (GSK2269557) (CAL101, Zydelig), the PDK1 inhibitor BX-795 and the FOXO1 inhibitor AS1842856 were bought from Selleckchem. The NIK inhibitor SMI1 was purchased from Hycultec. All inhibitors were dissolved in DMSO at 10–50 mM according to manufacturer's instructions. The human monoclonal IgG1λ anti-BAFF antibody Belimumab (benlysta) was purchased from GlaxoSmithKline Pharmaceuticals and hTACI (aa 31–110)-hIgG1 Fc (aa 245–470) (from plasmid ps3825) was prepared as described before (Kowalczyk-Quintas et al., 2019). Primary cells and cell lines were treated with the indicated concentration of inhibitors or the respective amount of DMSO for 1 h prior to stimulation with the ligands.

For B cell survival assay, purified total B cells (5 × 10<sup>4</sup>) were plated in round-bottomed 96-well plates and stimulated with BAFF (20 ng/mL). After 3 days, the cell numbers were determined by flow cytometry by timed acquisition, within a CD19<sup>+</sup> 4',6-diamidino-2-phenylindole (DAPI)<sup>-</sup> gate.

### **Flow cytometry**

Analyses of cell surface and intracellular proteins was performed using a FACS Canto II flow or Fortessa LSR cytometer (BD Biosciences); data were analyzed with the FlowJo v.10 software (BD Biosciences). Dead cell exclusion was performed by DAPI staining in living cells or Fixable Viability Dye eFluor450 (eBioscience) prior to fixation. Antibodies used for flow cytometry were from Biolegend, unless indicated otherwise.

PBMCs, isolated B cells or cell lines were stained on ice in PBS containing 5% FCS and 2 mM EDTA with the following antibodies: anti-CD19 APC-Cy7, anti-CD19 Pe/Cy7 (BD Biosciences), anti-BAFFR (PE, Alexa Fluor 647), anti-TACI (APC), anti-IgD (FITC, PE; SouthernBiotech), anti-IgD PerCP/Cy5.5, anti-IgM APC Cy-7, anti-IgM Cy5 (Jackson ImmunoResearch), anti-IgA Alexa Fluor 647 (Jackson ImmunoResearch), anti-IgA FITC (SouthernBiotech), anti-IgG Alexa Fluor 647 (Jackson ImmunoResearch), anti-IgG PE, anti-CD79A Alexa Fluor 488 (R&D systems), anti-CD79B (PE, APC), anti-CD27 (PE, PerCP/Cy5.5, Pe/Cy7, Brilliant Violet 421), anti-CXCR4 (Brilliant Violet 421), anti-CD54 APC, anti-CD62L APC, anti-CD69 PE, anti-CD83 PeCy5, anti-CD98 FITC, anti-IL21R PE, anti-GARP (LRRC32) Brilliant Violet 421, anti-CD172a/b (SIRPα/β) FITC, anti-kappa light chain FITC, anti-lambda light chain PE.

Intracellular proteins were detected in cells stained first with anti-CD27 antibodies at 4°C, followed by fixation with 4% paraformaldehyde and permeabilization with 0.1% saponin-PBS at room temperature (RT). Cells were then stained at RT with different antibody cocktails containing a combination of the following antibodies: anti-CD19 (APC-Cy7), anti-CD19 Pe/Cy7 (BD Biosciences), anti-IgD (FITC, PE; SouthernBiotech), anti-IgD PerCP/Cy5.5, anti-phospho-S6 (S240/S244) PE (Cell Signaling Technology), anti-Bcl2 PE, anti-IRF4 Pe/Cy7, anti-PTEN APC (MiltenyiBiotec), anti-CD79A PE (Beckman Coulter), anti-CD79A Alexa Fluor 647, anti-CD79B (un-labeled; Cell Signaling), anti-TCL1A APC (eBioscience). Proteins secreted by B cells were analyzed by blocking protein transport with the inhibitor Brefeldin A (Biolegend) for 4 h at 37°. Cells were then fixed, permeabilized and stained at RT with anti-IL-10 Alexa Fluor 488, anti-IL1β Alexa Fluor 647 or anti-IL-6 PerCP/Cy5.5 antibodies, washed once and resuspended in PBS containing 5% FCS and 2 mM EDTA for analysis. The anti-His Tag Alexa Fluor 647 and F(ab')<sub>2</sub> anti-rabbit IgG (H + L) Alexa Fluor 647 secondary antibodies were purchased from Biolegend and Jackson ImmunoResearch respectively. FCS files were analyzed with FlowJo gating for CD19<sup>+</sup> B cells, IgD<sup>+</sup> CD27<sup>-</sup> (naive) and (IgD<sup>-</sup> CD27<sup>+</sup>) memory B cells as shown in Figure S1.

### **Western blot analysis**

Whole cell lysates were prepared from purified B cell subsets and/or cell lines in Laemmli sample buffer as described previously (Pieper et al., 2014; Smulski et al., 2017). Protein extracts were separated by 8–12% SDS-PAGE and transferred onto 0.2-μm nitro-cellulose membranes (Cytiva). The following primary antibodies were used: anti-CD79A, anti-phospho-CD79A (Tyr182; corresponds to Tyr188 of the human homolog), anti-CD79B (clone D7V2F), anti-AKT (clone 40D4), anti-phospho-AKT (Ser473; clone D9E), anti-CD19, anti-phospho-CD19 (Tyr531), anti-PTEN (clone D4.3), anti-4E-BP1, anti-phospho-4E-BP1 (Ser65; clone 174A9), anti-phospho-SYK (Tyr525/526; clone C87C1), anti-phospho-S6 Ribosomal Protein (Ser240/244; clone D68F8), anti-FOXO1 (clone D7C1H), anti-MCL-1 (clone D35A5), anti-BCL-XL (clone 54H6), anti-phospho-Src family [Tyr416; corresponds to Tyr419 of human Src; clone D49G4), anti-phospho-LYN (Tyr507), anti-LYN (clone C13F9), anti-STAT5 (clone 3H7), anti-TRAF3 (clone D1N5B), all from Cell Signaling Technology (CST), anti-phospho-FOXO1 (Ser256; Thermo Fischer Scientific), anti-NFκB p52 (Millipore) and anti-β-actin (clone AC15; Sigma Aldrich), anti-BAFFR-CT (Enzo), anti-BAFFR (clone H1; Santa Cruz), anti-μ heavy chain (SouthernBiotech). Bound primary antibodies were detected with horseradish peroxidase-conjugated donkey anti-mouse, donkey anti-rabbit and donkey anti-goat secondary antibodies (Jackson ImmunoResearch). Membranes were developed with enhanced chemiluminescent detection reagents (SuperSignal West Pico PLUS chemiluminescent substrate from Thermo Fischer Scientific or Western Bright Sirius HRP substrate from Advansta). The signal intensities were quantified using ImageJ software (NIH).

### Co-immunoprecipitation

DG-75 cells ( $2 \times 10^7$ ) were rested for 30 min prior to stimulation with FLAG-tagged BAFF or left untreated. Cells were washed once with ice-cold PBS and lysed on ice in lysis buffer containing 20 mM Tris-HCl (pH 7.4), 150mM NaCl, 0.2% NP-40, 10% glycerol, complete protease inhibitor cocktail for 15 min. Cell lysates were centrifuged at 13,000 rpm for 10 min at 4°C to pellet nuclei. Supernatants were incubated overnight at 4°C under constant agitation with anti-FLAG agarose beads (anti-FLAG M2 Affinity gel, Thermofisher) which were previously washed and equilibrated in lysis buffer. Samples were loaded to mini-columns as described in (Schneider et al., 2014), washed twice with lysis buffer (containing 350 mM NaCl) and bound immunocomplexes were eluted with citrate buffer (pH 2.4) before neutralizing in 1.5 M Tris buffer (pH 9). Eluted proteins were mixed with 4× Laemmli sample buffer, boiled for 5 min at 95°C and loaded in 10% PAGE-SDS for western blot analysis.

### Flow cytometry-based FRET

Flow cytometry based FRET was carried out as described in (Schneider et al., 2014). DG-75 BAFFR KO cells (IgM<sup>+</sup> or IgD<sup>+</sup> or IgA<sup>+</sup> or IgG<sup>+</sup>) were transduced with lentiviral vectors encoding full-length proteins that were C-terminally fused to eCFP, eYFP or RFP (BAFFR-CFP, CD79A- and CD79B-YFP or RFP). FACS-FRET measurements were performed using a LSRII Fortessa flow cytometer (BD Biosciences). The donor fluorophore eCFP (BAFFR-eCFP) was excited with a 405 nm laser and fluorescence was detected with a 470/24 BP emission filter, the acceptor fluorophore (eYFP; CD79A-eYFP or CD79B-eYFP) was excited with a 488 nm and detected with a 530/30 BP filter, and the second acceptor fluorophore (RFP; CD79A-RFP or CD79B-RFP) was excited with a 561 nm laser and detected with a 586/15 BP filter. The CFP/YFP FRET was measured with a 550/15 BP emission filter and the CFP/RFP FRET with a 610/20 BP emission filter (both with a 405 nm excitation); YFP/RFP FRET was recorded with a 625/15 BP emission filter (with a 488 nm excitation). Single-positive cells were used as background controls. For each sample, we analyzed  $\geq 5000$  eCFP/eYFP/RFP triple-positive cells. To evaluate changes upon ligand binding,  $0.1 \times 10^6$  cells/100  $\mu$ L were stimulated for 6 h with BAFF (100 ng/mL) or F(ab')<sub>2</sub> goat anti-human IgM (2  $\mu$ g/mL) or left untreated. Cells were washed (256 × g, 5 min, RT), resuspended in Fluorobrite DMEM Medium (Thermo Fischer Scientific) supplemented with 10% FCS and analyzed.

### RNA extraction and RNA sequencing

Naive and switched-memory B cells from 4 healthy donors (biological replicates) were isolated by negative selection as described above. Cells ( $1 \times 10^6$ ) were incubated in a 24-well plate in the presence or absence of BAFF (20 ng/mL). From one donor (L8), two technical replicates of naive B cells were processed. After 6 h, cells were collected and washed twice with sterile PBS. Total RNA was extracted from cell pellets with the Qiagen RNeasy Mini kit according to manufacturer's instructions. A complementary DNA library was prepared using the TruSeq Standard Total RNA kit, and sequencing was performed with NovaSeq6000 according to the Illumina standard protocol by Beijing Novel Bioinformatics Co., Ltd using a paired-end 150-bp sequencing strategy. The 18 samples (5 naive B cells ± BAFF, 4 memory B cell samples ± BAFF) were processed using two Nextflow (Di Tommaso et al., 2017) pipelines: CLEAN (<https://github.com/hoelzer/clean>) for removal of rRNA reads followed by RNAflow (Lataretu and Hölzer, 2020) for differential gene expression. The rRNA reads were removed with CLEAN using BBDuk (v38.79) (<https://sourceforge.net/projects/bbmap>). Then, RNAflow guided through the next steps starting from quality control of raw data, read alignment, gene quantification, normalization, differential expression calling, and visualization of results. In short, samples were quality checked with FastQC (v0.11.9) (<https://www.bioinformatics.babraham.ac.uk/projects/fastqc>) and raw reads were trimmed using FASTP (Chen et al., 2018) to remove low-quality bases and adaptor contaminants. Processed reads were aligned with HISAT2 (Kim et al., 2015) to the human primary reference genome GRCh38 obtained from Ensembl. Gene-level expression quantification was performed with featureCounts (v2.0.1) (Liao et al., 2014). In addition, TPM (transcripts per million) values were calculated by RNAflow to identify and discard weakly expressed genes (TPM  $\leq 1$ ). Finally, differential gene expression analysis of grouped samples (naive vs MBC, ± BAFF) was performed with DESeq2 (Love et al., 2014). Principal component analysis (PCA) and heatmaps were generated by R packages implemented in the RNAflow pipeline. In addition, we explored the PCA results using the PCAGO web service (<https://pcago.bioinf.uni-jena.de>) (Gerst and Hölzer, 2019).

### Assembly of the ribonucleoprotein (RNP) complexes and electroporation of cells

CRISPR RNAs (crRNAs) targeting *CD79A*, *CD79B*, *IGHM*, *LYN*, *CD27*, *TNFRSF13C*, *TCL1A* and *TNFRSF13B* were designed with the aid of DeskGen (<http://www.deskgen.com>), CHOPCHOP (<https://chopchop.cbu.uib.no/>) and the Integrated DNA Technologies (IDT) crRNA design tool (<https://eu.idtdna.com/>). The gRNA oligonucleotides were synthesized by the Integrated DNA Technologies. The sequences of the gRNAs are as follows (the protospacer adjacent motif sequence is underlined):

*CD79A* gRNA: TCCTCCATGGCAACTACACGTGG.  
*CD79B* gRNA: AACACCTCGGAGGTCTACCAGGG.  
*IGHM* gRNA: CCTTCCAAGGACGTATGCAGGGC.  
*LYN* gRNA: TTAATAACATCACCATGCACAGG.  
*TNFRSF13C* gRNA: CTCACCGTCCTTGCTCCGTCG.  
*CD27* gRNA: GTTTGGAAGAGGATCACACTCGG.  
*TCL1A* gRNA: CAAATACACGAACTTCTCCCAGG.  
*TNFRSF13B* gRNA: CTCGGAAGGTACCAAGGATTGG

crRNA and tracer RNAs (tracrRNA) (IDT) of 200  $\mu\text{M}$  were mixed at equimolar concentrations and incubated at 95°C for 5 min to form guide RNAs (gRNA) at a concentration of 44  $\mu\text{M}$ . Next, the mix was cooled slowly to RT and the gRNA was mixed in a 1:1 ratio by volume with 36  $\mu\text{M}$  of Cas9 enzyme and incubated for 20 min at RT for the formation of the RNP complex.

Primary B cells and the DG-75 cell line were electroporated with the Neon Transfection system 10  $\mu\text{L}$  kit (Thermo Fischer Scientific). Freshly isolated primary B cells or the DG-75 cells ( $5 \times 10^5$ ) were collected by centrifugation, washed twice with PBS, and resuspended in 9  $\mu\text{L}$  electroporation buffer (T for primary cells or R for cell lines). The cell suspension was added to the RNP complex and mixed with 10.8  $\mu\text{M}$  electroporation enhancer (IDT). Cells were then loaded in 10  $\mu\text{L}$  tips and electroporated at 1450V or 2150V (for cell lines and primary B cells, respectively), 20 ms width, and 1 pulse. After electroporation, cells were plated in IMDM supplemented with 20% FCS without antibiotics for 2 days until they were used for further assays.

### QUANTIFICATION AND STATISTICAL ANALYSIS

Data analysis was performed with Prism 8.4 software (Graphpad). For all statistical comparisons with more than two groups, the data were analyzed with one-way Anova (Kruskal-Wallis  $H$  test or Mann-Whitney-U test) or two-way Anova with Tukey's or Sidak's multiple comparisons test. Differences between groups were considered significant when  $p < 0.05$  (ns  $p > 0.05$ ; \* $p = 0.01$  to 0.05; \*\* $p = 0.001$  to 0.01; \*\*\* $p = 0.0001$  to 0.001; \*\*\*\* $p < 0.0001$ ).

**Supplemental information**

**BAFFR activates PI3K/AKT signaling in human naive  
but not in switched memory B cells through direct  
interactions with B cell antigen receptors**

**Eirini Sevdali, Violeta Block, Marie Lataretu, Huiying Li, Cristian R. Smulski, Jana-Susann Briem, Yannic Heitz, Beate Fischer, Neftali-Jose Ramirez, Bodo Grimbacher, Hans-Martin Jäck, Reinhard E. Voll, Martin Hölzer, Pascal Schneider, and Hermann Eibel**

Supplemental Figures

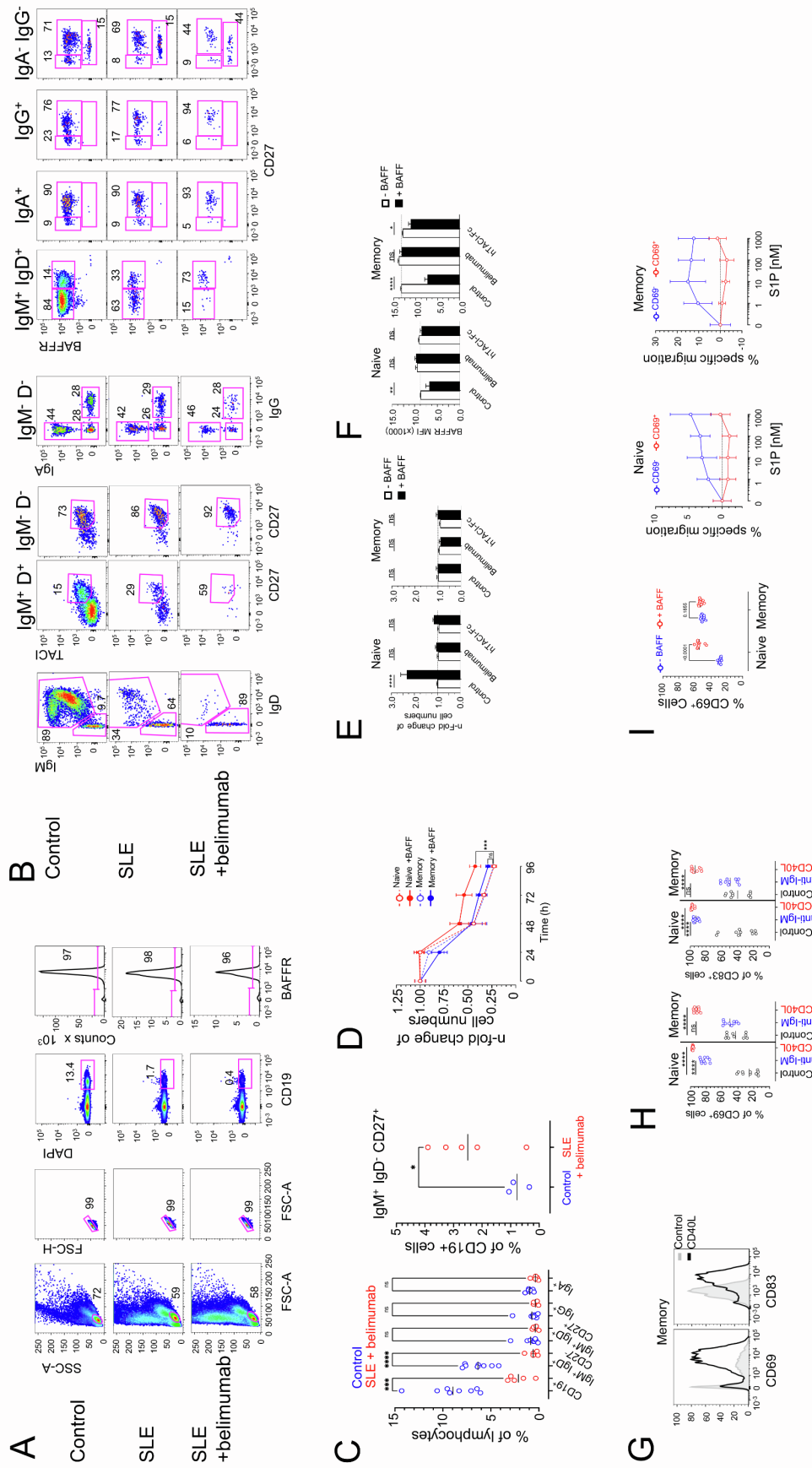


**Figure S1 (related to Figure 1). Phenotype, BAFF-dependent survival and activation of B cell subsets.**

**A. Gating strategy applied in flow cytometric analyses.** The representative example shows lymphocyte populations of peripheral blood mononuclear cells (PBMCs) from a healthy donor (control), a SLE patient (SLE) and a SLE patient treated for > 1 year with belimumab as identified by the forward (FSC-A) and the side scatter (SSC-A) reflecting the small size and low granularity of these cells. Within the lymphocyte population, single cells were gated by the FSC-A (area) and FSC-H (height). Living B cells were defined as CD19<sup>+</sup> DAPI<sup>-</sup> cells, of which > 96% expressed BAFFR.

**B. B cell subsets.** The CD19<sup>+</sup> cells of the control, SLE and SLE + belimumab samples were analyzed for the expression of IgM, IgD, CD27, BAFFR, TACI, IgA and IgG. The IgM<sup>+</sup> IgD<sup>+</sup> subset included naive (IgD<sup>+</sup> CD27<sup>-</sup>) and marginal zone B cells (IgD<sup>+</sup> CD27<sup>+</sup>). The latter expressed TACI on their cell surface. Most of the IgM<sup>-</sup> IgD<sup>-</sup> cells were switched memory B cells (MBCs) expressing IgA (IgA<sup>+</sup>, 42 - 46%) or IgG (IgG<sup>+</sup>, 28 - 29%), CD27 and TACI (73 - 92%). CD19<sup>+</sup> IgM<sup>-</sup> IgD<sup>-</sup> IgG<sup>-</sup> IgA<sup>-</sup> cells (24 - 28%) were BAFFR<sup>+</sup> (53 - 84%) or BAFFR<sup>low/+</sup> CD27<sup>low/+</sup> (15 - 44%).

**C. Memory B cells persist in belimumab-treated SLE patients.** Lymphocytes of controls and SLE patients who were treated with belimumab for > 6 months were gated as shown in panels A and B and analyzed by flow cytometry for the expression of CD19, CD27, IgM, IgD, IgG, and IgA. The plot on the left compares the percentages of B cells and B cell subsets in lymphocytes of controls (n=8) and belimumab-treated SLE patients (n=5). Controls have significantly more CD19<sup>+</sup> B cells and CD19<sup>+</sup> IgD<sup>+</sup> CD27<sup>-</sup> naive B cells than SLE patients treated for > 6 months with the BAFF-neutralizing mAb belimumab. The plot on the right side

shows the percentages of IgM<sup>+</sup> IgD<sup>-</sup> CD27<sup>+</sup> memory B cells in controls (n=3) and in the SLE patients (n=5). Statistically significant differences between controls and patients were calculated applying Brown-Forsythe and Welch's ANOVA assuming unequal SD with Dunnett T3 correction for multiple comparisons with n<50. (\*p≤0.0332; \*\*p≤0.0021; \*\*\*p≤0.0002; \*\*\*\* p<0.0001; ns, not significant).

**D. BAFF-induced survival in naive and memory B cells.** B cells were stimulated with BAFF (20 ng/ml) for 4 sequential days and analyzed by flow cytometry and timed acquisition. N-fold changes of cell numbers were calculated as [cell number at each day ±BAFF /cell number –BAFF at day 0]. Plots show the mean and SD of 2 independent experiments (3 replicates/experiment) with two healthy donors (HD); \*\*\*p<0.001; ns, not significant (Kruskal-Wallis with Dunn's multiple comparisons test).

**E. B cells do not produce endogenous BAFF.** BAFF (20 ng/mL) was mixed with belimumab (1 µg/mL), hTACI-Fc (100 ng/mL) or medium (control) and incubated at room temperature for 1 day. B cells were then incubated with BAFF ±belimumab or ±TACI-Fc for 3 days or without the ligand, and cell numbers were analyzed by flow cytometry and timed acquisition. N-fold changes in cell numbers were calculated as [cell number ± BAFF ± inhibitor]/[cell number without BAFF without inhibitor]. The plots show the mean ±SEM of n-fold change of cell counts of each B cell subset from two independent experiments with samples from two different HD. \*\*\*\*p<0.0001; ns, not significant (2-way Anova with Tukey multiple comparisons test).

**F. Belimumab and hTACI-Fc block BAFF binding to BAFFR.** Median fluorescence intensity (MFI) of BAFFR surface expression of naive and memory B cell subsets shown in (E) at day 3 using the anti-BAFFR monoclonal antibody

11C1. The antibody binds to BAFFR only when BAFFR is not occupied by BAFF. The plot shows the mean  $\pm$ SEM of BAFFR MFI from two independent experiments with two different HD; \*\*\*\* $p < 0.0001$ ; \*\* $p < 0.01$ ; \* $p < 0.05$ ; ns, not significant (2-way Anova with Tukey multiple comparisons test).

**G. CD40L induces CD69 and CD83 expression in memory B cells.** Histogram overlays show changes in CD69 and CD83 expression by MBCs activated with CD40L overnight. The histogram plots are representative of 6 independent experiments with B cells from different healthy donors.

**H. Anti-IgM and CD40L differentially activate CD69 and CD83 expression in naive and memory B cells.** CD40L induces CD69 and CD83 expression on the surface of naive and of MBCs, while anti-IgM activates only naive B cells. B cells were incubated overnight with anti-IgM (2  $\mu$ g/mL) or CD40L or left untreated and analyzed by flow cytometry. Plot shows the mean of pooled data from 6 independent experiments with B cells from different HD. \*\*\*\* $p < 0.0001$ ; ns, not significant (2-way Anova with Tukey multiple comparisons test).

**I. BAFF-induced CD69 inhibits S1P-dependent B cell migration.** B cells were cultivated overnight with BAFF or left untreated. The migration against S1P was then analyzed in transwell assays with different concentrations of S1P in the lower well. Cells in upper and lower wells were analyzed by flow cytometry for the expression of IgD, CD27 and CD69. The fraction of sessile or migrating cells was determined by timed acquisition. The percentage of migrating cells was calculated as  $[\text{number of cells isolated from the lower well}] / [\text{number of cells retrieved from the upper well}] \times 100$ . The transwell migration assay was performed with two biological and two technical replicates. Plots show mean values  $\pm$ SD. Statistical significances in CD69 expression between naive and

memory B cells were calculated by 2-way ANOVA with Tukey multiple comparisons test.



**Figure S2 (related to Figure 2). Gene expression patterns.**

**A. Normalized counts of transcripts in naive and memory B cells.** The box plots show transcripts of genes expressed typically by naive and MBCs, or by plasma cells. IGHM and IgHD are expressed by naive and MZ B cells, the H-chain genes of the switched isotypes (IGHG1 – IGHG4, IGHA1, IHGA2) by memory B cells, BAFFR is expressed by all B cells, CD23 preferentially by naive B cells, CD27, TACI and Fas by memory B cells, BCMA and PRDM1 are expressed by plasma cells. The box plots represent normalized gene expression values showing the spread as boxes, the mean as lines (numerical values) and the individual values as dots.

**B. Scatter plot of RNA-seq expression analysis.** The scatter plot shows log<sub>2</sub> fold-changes in response to BAFF of differentially expressed genes present in both comparisons (naive B cells +BAFF vs naive B cells –BAFF vs memory B cells –BAFF vs naive B cells –BAFF). Significant differentially expressed genes adjusted to p-values <0.1 in both comparisons are colored in red. Green and blue show transcripts that are expressed with significant differences in only one comparison, memory B cells –BAFF vs naive B cells –BAFF, and naive B cells +BAFF vs naive B cells –BAFF, respectively.

**C. Volcano plots of the RNA-seq expression analysis.** Volcano plot representation of genes significantly regulated by BAFF in naive (left) and in memory B cells (right); log-fold-change threshold = 0.9, adjusted p-value = 0.1.

**D. Functional (indirect) and direct interactions of genes upregulated by BAFF in naive B cells.** The networks showing interactions between genes induced or repressed were generated with STRING, a database of known and

predicted protein-protein interactions (<https://www.string-db.org>). The parameters were set for full networks based on evidence (textmining, experiments, databases, co-expression) applying a high confidence score of 0.70. Clusters were calculated by K-means clustering to a specific number of 5.

**E. Functional (indirect) and direct interactions of genes downregulated by BAFF in naive B cells.** The networks were identified by STRING as described in panel D.

**F. BAFF-induced change in the expression of chemokines and interleukins.** Purified B cells were incubated for 2 days with BAFF (20 ng/mL) or left untreated and analyzed for the expression of CCL3, CCL4, IL-1 $\beta$ , IL-6 and IL-10 by intracellular flow cytometry.

**G. BAFF induces IL-21R expression on naive B cells and stimulates proliferation in the presence of IL-21.** B cells were labelled with cell-trace violet (CTV) and stimulated with BAFF, CD40L or left untreated for 4 days. The plot shows the MFI of IL21R surface expression in naive and MBCs from 2 independent experiments (left). The percentage of dividing cells was calculated by the dilution of CTV by B cells treated for 2 days with BAFF or CD40LG followed by the addition of IL-21 for 2 days. The histogram inserts show the dilution of the CTV label after 4 days of cultivation. Black histogram = control, red = BAFF + IL-21, blue = CD40L + IL-21.

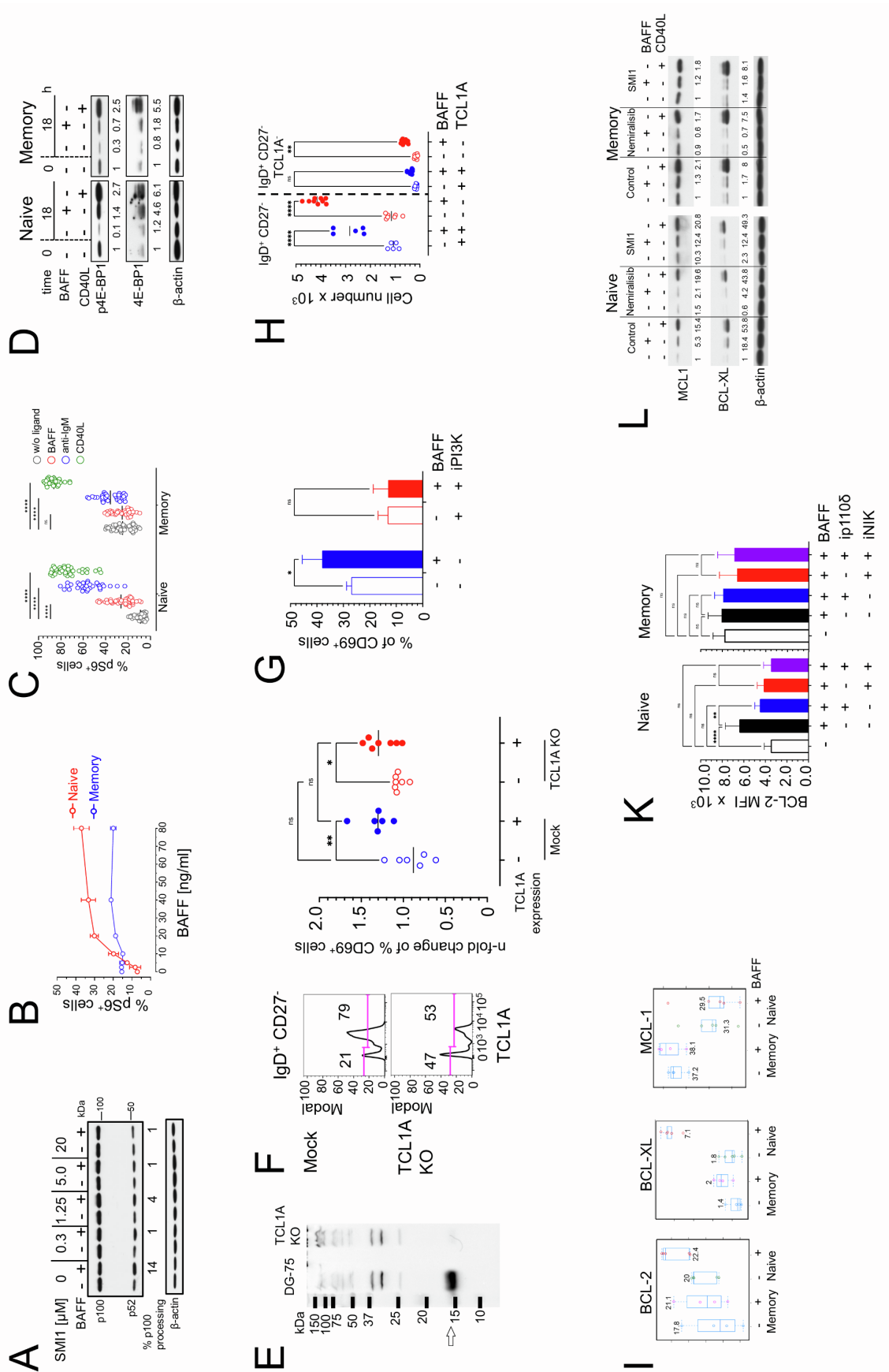


**Figure S3 (related to Figure 3). BAFFR signaling in naive and switched memory B cells.**

**A. Inhibition of NIK blocks BAFF-induced NF- $\kappa$ B2 processing in primary B cells.**

B cells were incubated with increasing concentrations of the cell-permeable NIK inhibitor SMI1 for 1 h before adding BAFF (20 ng/mL). After overnight incubation, whole extracts were analyzed by immunoblotting for the NIK-dependent processing of NF- $\kappa$ B2 p100 precursor into p52. The percentage of NF- $\kappa$ B2 processing (% p100 processing) was calculated after densitometric analysis of the western blot images as  $[100 \times (\text{p52 signal})/(\text{p52}+\text{p100 signal})][+\text{BAFF}] - 100 \times (\text{p52 signal})/(\text{p52}+\text{p100 signal})[\text{w/o BAFF}]$ .

**B. BAFF-induced S6 phosphorylation differs between naive and memory B cells.**

Peripheral blood mononuclear cells (PBMCs) were treated with increasing concentrations of BAFF for 1 h and the phosphorylation of S6 (S240/244) was assessed by intracellular flow cytometry. The diagram displays mean percentage  $\pm$ SEM of pS6<sup>+</sup> cells within the naive and memory B cell subsets of two healthy donors.

**C. Comparison of S6 phosphorylation induced by BAFF, anti-IgM or CD40L.**

PBMCs were treated with BAFF, F(ab')<sub>2</sub> anti-IgM (2  $\mu$ g/mL) or CD40L for 1 h and analyzed for the phosphorylation of S6 (S240/244) as described in (B). The plot shows the mean of pS6<sup>+</sup> cells within the naive and memory B cell subsets from at least 5 healthy donors analyzed in duplicates - quadruplicates. \*\*\*\*p<0.0001; ns, not significant (2-way Anova with Tukey multiple comparisons test).

**D. BAFF induces phosphorylation of the translational repressor 4E-BP1 in naive but not in memory B cells.**

Naive and memory B cells were treated with

BAFF or CD40L overnight. Whole cell extracts were immunoblotted with antibodies against total and phosphorylated 4E-BP1 (S65). Data are representative of one out of two independent experiments. N-fold changes in p4E-BP1 and 4E-BP1 levels were calculated as signals normalized to actin and further normalized to the untreated sample from day 0 for each B cell subset.

**E. *TCL1A* inactivation in DG-75 cells.** DG-75 cells were electroporated with a gRNA-Cas9 RNP complex targeting the exon 1 of the *TCL1A* locus. Total *TCL1A* protein expression in the parental DG-75 cells and *TCL1A* KO cells was assessed by western blotting. The position of *TCL1A* in the western blot is marked by the arrow.

**F. *TCL1A* inactivation impairs BAFF-induced upregulation of CD69.** *TCL1A* was inactivated in primary B cells as in DG-75 (shown in E). Two days after the electroporation, cells were incubated with BAFF (20 ng/mL) or without for one day and analyzed for the expression of CD69 by IgD<sup>+</sup> CD27<sup>-</sup> naive B cells. The histogram plots show the percentage of *TCL1A*-negative cells, which increased from 21% in mock electroporated cells to 47% in B cells electroporated with *TCL1A* gRNA/Cas9 RNPs. The graph shows the n-fold changes in the percentages of CD69<sup>+</sup> cells in response to BAFF treatment of *TCL1A*-negative and *TCL1A*-positive, mock-electroporated or *TCL1A*-inactivated cells after one day of cultivation ± BAFF. BAFF did not induce CD69 expression in *TCL1A*<sup>-</sup> naive B cells. The experiment shows 2 - 4 independent replicates of two different donors. Significant differences were calculated by two-tailed Brown-Forsythe and Welch ANOVA for multiple comparisons assuming unequal SDs (ns = not significant. \* p<0.0332; \*\* p<0.0002; ns, not significant).

**G. Inhibition of PI3K reduces upregulation of CD69.** IgD<sup>+</sup> CD27<sup>-</sup> naive B cells were cultivated overnight without or with BAFF in the presence of the PI3K inhibitor nemiralisib (iPI3K, 1  $\mu$ M) or DMSO and analyzed for the surface expression of CD69 by flow cytometry. The plot shows the mean  $\pm$ SD of the percentage of CD69<sup>+</sup> cells within the naive subset. \* $p$ <0.05; ns: not significant (2-way ANOVA with Sidak's multiple comparisons test).

**H. *TCL1A* inactivation does not change BAFF-induced survival.** *TCL1A* was inactivated in B cells as described in the legend of panel E. Two days post electroporation, cells were cultivated without or with BAFF (20 ng/ml) for 3 additional days. Survival of total and *TCL1A*<sup>-</sup> IgD<sup>+</sup> CD27<sup>-</sup> naive cells was analyzed by flow cytometry and timed acquisition. The experiment was performed in 5 - 9 technical replicates. \*\*\*\* $p$ <0.0001; \*\* $p$ <0.01; ns, not significant (2-way ANOVA with Tukey multiple comparisons test).

**I. *BCL-2*, *BCL-XL* and *MCL-1* mRNA levels in naive and memory B cells.** B cell subsets were cultivated for 6 h with BAFF (20 ng/mL) or left untreated; transcript levels were analyzed by RNA-Seq as described in Figure 2. The box plots represent the normalized gene expression values showing the spread as boxes, means as lines, and the individual values as dots. The numerical values correspond to the means.

**K. Inhibition of PI3K and NIK prevents BAFF-induced *BCL-2* expression in naive B cells.** B cells were cultivated for 2 days with BAFF (20 ng/mL) in the presence of inhibitors against PI3K $\delta$  (nemiralisib, 0.625  $\mu$ M), NIK (SMI1, 10  $\mu$ M) or DMSO (control) and analyzed for *BCL-2* expression by intracellular flow cytometry. The plot shows the mean and SEM of *BCL-2* MFI in naive and MBCs from two independent experiments with two different HD and technical duplicates.

\*\*\*\* $p < 0.0001$ ; \*\* $p < 0.01$ ; ns, not significant (2-way ANOVA with Tukey multiple comparisons test).

**L. PI3K inhibition interferes with BAFF-induced expression of anti-apoptotic proteins MCL-1 and BCL-XL in naive B cells.** Western blot analysis of MCL-1 and BCL-XL in naive and memory B cells after an overnight stimulation with BAFF or CD40L in the presence of inhibitors against PI3K $\delta$ , NIK or DMSO (control). The immunoblot shows the representative data from one out of two independent experiments. N-fold change of MCL-1 and BCL-XL expression was calculated as signals normalized to actin and further normalized to the untreated sample for each B cell subset.

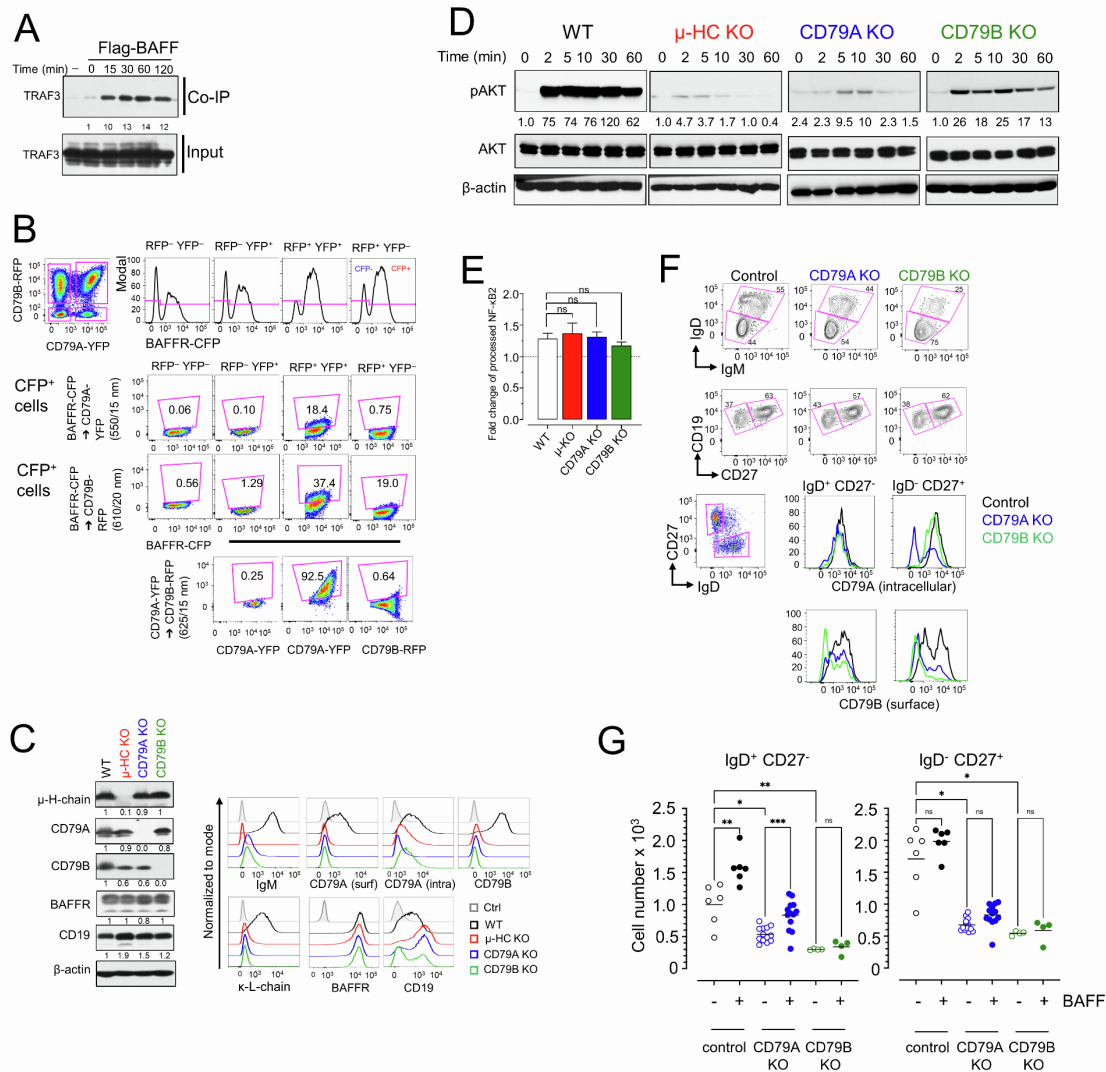


**Figure S4 (related to Figure 5). Interactions with BCR components regulate BAFFR signaling.**

**A. FLAG-BAFF co-immunoprecipitates TRAF3.** DG-75 cells were incubated with FLAG-tagged BAFF for 15 - 120 min at 37°C or at 0°C for 5 min (t = 0). Cells were lysed and immunocomplexes were precipitated with anti-FLAG M2-coupled agarose beads followed by western blot analysis of TRAF3. Lysates of untreated cells were used as control (-) to determine non-specific binding of proteins to the beads. N-fold change in TRAF3 recruitment was calculated as signals normalized to TRAF3 in input samples and further normalized to t = 0.

**B. Gating strategy to detect FRET<sup>+</sup> cells.** BAFFR-KO DG-75 Burkitt's lymphoma cells were transduced with lentiviral vectors encoding BAFFR-CFP, CD79A-YFP and CD79B-RFP fusion proteins. The transduction resulted in 4 populations according to YFP/RFP expression: RFP<sup>+</sup> cells, YFP<sup>+</sup> cells, YFP<sup>+</sup> RFP<sup>+</sup> cells and YFP<sup>-</sup> RFP<sup>-</sup> cells. Based on the expression of BAFFR-CFP, each subset was divided into CFP<sup>+</sup> and CFP<sup>-</sup> cells (histogram plots of upper row, RFP<sup>+</sup> YFP<sup>-</sup>, RFP<sup>+</sup> YFP<sup>+</sup>, RFP<sup>-</sup> YFP<sup>+</sup> and RFP<sup>-</sup> YFP<sup>-</sup> cells showing expression of BAFFR-CFP). FRET from CFP to YFP or from CFP to RFP was detected in the CFP<sup>+</sup> subsets, whereas FRET from YFP to RFP was only detected in the YFP<sup>+</sup> RFP<sup>+</sup> population. Excitation of CFP with the 405 nm laser induced fluorescence resonance energy transfer from CFP to YFP which was detected using a 550/15 nm bandpass filter (BAFFR-CFP → CD79A-YFP 550/15 nm). Energy transfer from CFP excited by the 405 nm laser to RFP was detected by signals passing a 610/20 nm bandpass filter (BAFFR-CFP → CD79B-RFP 610/20 nm). Energy transfer from YFP excited by 488 nm laser to RFP was detected using an 625/15 nm band pass filter (bottom row). Cell populations which did not express the respective FRET partner protein (YFP<sup>-</sup> RFP<sup>-</sup> cells, YFP<sup>+</sup> RFP<sup>-</sup> cells and RFP<sup>+</sup> YFP<sup>-</sup> cells) were used to set the gates for FRET<sup>+</sup> cells. In particular, to detect FRET from CFP to YFP or RFP, CFP<sup>+</sup> YFP<sup>-</sup> RFP<sup>-</sup> cells were used to set the gates for signals passing the 550/15 nm and the 610/20 nm filters, while the CFP<sup>-</sup> YFP<sup>+</sup> RFP<sup>-</sup> cells were used to set the gate for signals passing the 625/15 nm filter.

**C. CD79A-, CD79B- and  $\mu$ -H chain KO DG-75 cells.** Western blot analysis of whole cell lysates from wild-type (WT),  $\mu$ -H-chain ( $\mu$ -HC), CD79A and CD79B KO cells showing total expression of  $\mu$ -H-chain, CD79A, CD79B, BAFFR and CD19;  $\beta$ -actin was used as a loading control; n-fold differences in protein expression

were calculated as signals normalized to actin and further normalized to the WT DG-75 cells (left panels). Flow cytometric analysis of surface expression of IgM, CD79A, CD79B, kappa light chain, BAFFR, CD19 and intracellular expression of CD79A in the WT,  $\mu$ -H-chain, CD79A and CD79B KO DG-75; control = unstained cells (right panels).

**D. Time course of AKT phosphorylation (S473) in response to anti-IgM treatment in WT,  $\mu$ -H-chain, CD79A and CD79B KO DG-75 cells.** Cells were treated with F(ab')<sub>2</sub> anti-IgM (2  $\mu$ g/mL) for 2 - 60 min. Whole cell extracts were analyzed by western blot using antibodies against pAKT (S473), total AKT and  $\beta$ -actin (loading control), showing that loss of CD79A, CD79B or  $\mu$ -H chain prevents AKT phosphorylation. Data are representative of 1 out of at least 5 independent experiments. N-fold changes were calculated relative to the t=0 sample of WT DG-75 cells.

**E. NF- $\kappa$ B2 activation in CD79A, CD79B and  $\mu$ -H-chain KO DG-75 cells.** DG-75 (WT), CD79A, CD79B and  $\mu$ -H-chain KO cells were pre-treated overnight with an inhibitor against NIK (10  $\mu$ M) to reduce the basal NF- $\kappa$ B2 processing. Then, the inhibitor was washed out and the cells were stimulated with BAFF (100 ng/mL) overnight in inhibitor-free medium. The next day, whole cell lysates were prepared to detect NF- $\kappa$ B2 processing by western blot. The percentage of processed NF- $\kappa$ B2 was calculated as  $[(\text{signal of p52})/(\text{signal of p52} + \text{signal of p100})] \times 100$ . The plot depicts the mean and SEM of n-fold changes in processed NF- $\kappa$ B2 after the addition of BAFF in the different cell lines from at least 3 independent experiments with 2 technical replicates. ns, not significant (Kruskal-Wallis test with Dunn's correction).

**F. Gene inactivation of *CD79A* and *CD79B* in primary human B cells.** *CD79A* and *CD79B* were inactivated by Cas9-directed mutagenesis in purified B cells with *CD79A* and *CD79B* gRNA-Cas9 RNPs. Equal numbers of cells were distributed into technical replicates, cultivated for 5 days and analyzed by flow cytometry and timed acquisition. Analysis of CD19<sup>+</sup> cells for IgM, IgD, and CD27 expression revealed a decrease in IgM and IgD surface levels after inactivation of *CD79A* and *CD79B* (contour plots). The inactivation of *CD79A* also reduced the surface expression of *CD79B* in both IgD<sup>+</sup> CD27<sup>-</sup> and IgD<sup>-</sup> CD27<sup>+</sup> cells. The pseudocolor plot shows the gating and the histogram overlays of *CD79A* and *CD79B* expression in mock electroporated controls (black), in *CD79A* KO (blue) and *CD79B* KO B cells (green).

**G. BAFF does not rescue B cells after inactivation of *CD79B*.** B cells were electroporated with gRNA/Cas9 RNPs targeting *CD79A* (blue symbols) or *CD79B* (green symbols), or without RNP complex (control, black symbols). Two days post electroporation, cells were cultivated ±BAFF (20 ng/ml) and analyzed by flow cytometry and timed acquisition after 3 additional days. The plots show the cell numbers of IgD<sup>+</sup> CD27<sup>-</sup> and IgD<sup>-</sup> CD27<sup>+</sup> cells from 2 HD (≥4 independent replicates). Because the inactivation of *CD79A* is less efficient than the inactivation of *CD79B*, some of the naive B cells in the *CD79A* KO samples are rescued by BAFF. The number of mock-electroporated or of *CD79A* or *CD79B* KO IgD<sup>-</sup> CD27<sup>+</sup> MBCs did not change in response to BAFF. \*\*\*p<0.0002; \*\*p<0.0021; \*p<0.0332; ns, not significant (Brown-Forsythe and Welch's ANOVA test for multiple comparisons).

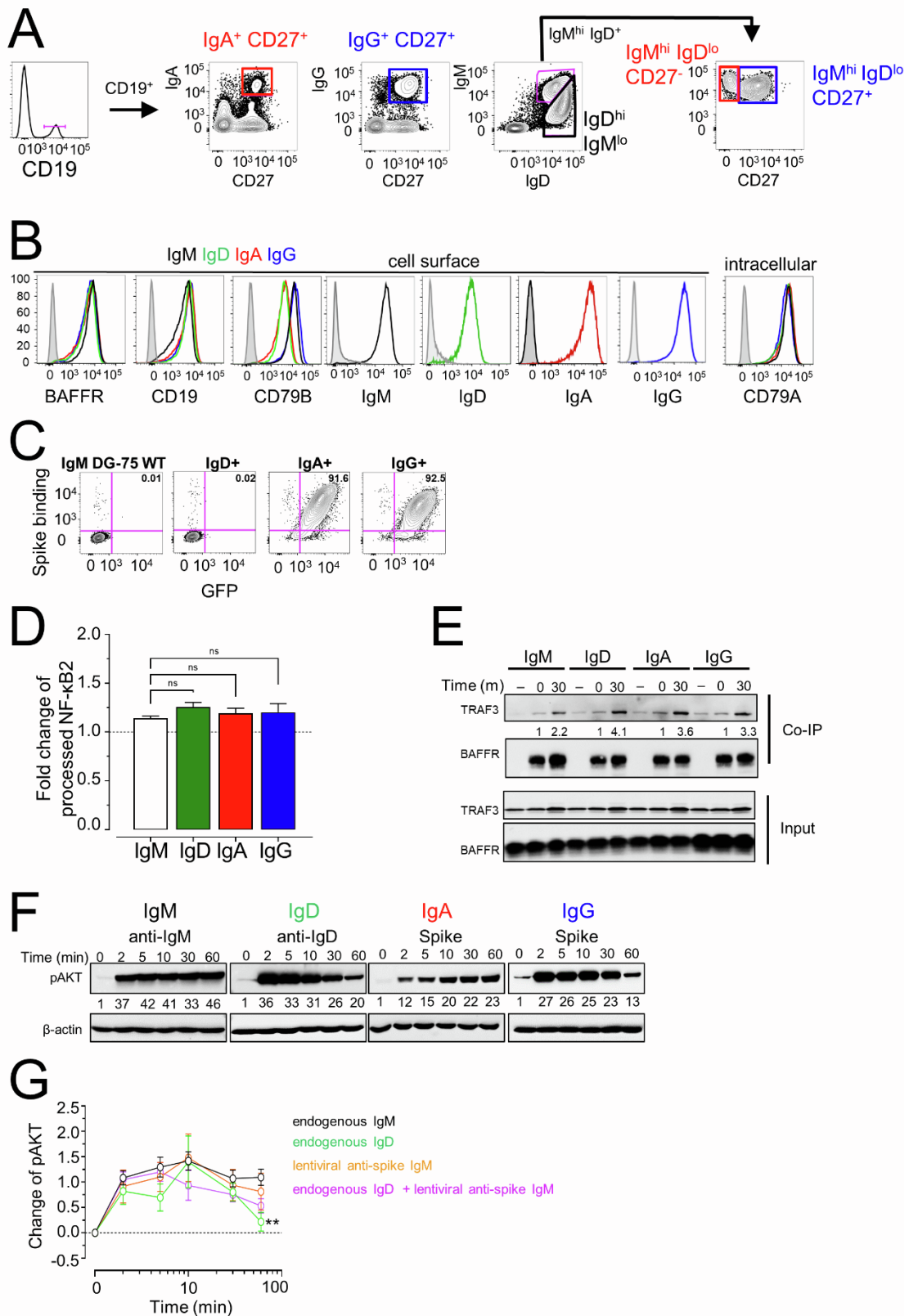


**Figure S5 (related to Figure 6). The BCR isotype restricts BAFF-induced PI3K activation in naive B cells.**

**A. Flow cytometric analysis of B cell subsets expressing different immunoglobulin isotypes.** CD19<sup>+</sup> cells were gated according to the expression of IgM, IgD, IgG, IgA and CD27 into IgD<sup>hi</sup> IgM<sup>low</sup> CD27<sup>-</sup>, IgD<sup>low</sup> IgM<sup>hi</sup> CD27<sup>-</sup>, IgD<sup>low</sup> IgM<sup>hi</sup> CD27<sup>+</sup>, IgA<sup>+</sup> CD27<sup>+</sup>, and IgG<sup>+</sup> CD27<sup>+</sup> subsets and analyzed by flow cytometry for the surface expression of Ig-kappa and Ig-lambda light chains shown in Figure 6.

**B. Surface expression of BAFFR, CD19, CD79B, IgM, IgD, IgA, IgG and intracellular expression of CD79A in DG-75 cell lines with different BCR isotypes.** Grey histogram = unstained cells.

**C. Binding of SARS-CoV-2 spike antigen to DG-75 cell lines expressing anti-spike IgA or IgG.** DG-75 WT (IgM<sup>+</sup>), IgD<sup>+</sup>, anti-spike IgA1<sup>+</sup> and IgG1<sup>+</sup> DG-75 cell lines (GFP<sup>+</sup>) were incubated with His-tagged-SARS-CoV-2 spike protein (1 µg/mL) for 30 min on ice. Cells were washed and further incubated with an anti-His tag Alexa Fluor 647-conjugated antibody for 30 min on ice. Cells were washed and analyzed by flow cytometry.

**D. NF-κB2 activation in DG-75 cells expressing different BCR isotypes.** Cells were treated overnight with an inhibitor against NIK (10 µM) to reduce the basal NF-κB2 processing. The day after, the inhibitor was washed out and the cells were treated with BAFF (100 ng/mL) overnight in inhibitor-free medium. The next day, whole cell lysates were prepared and NF-κB2 processing was analyzed by western blot. Signal intensities were determined by densitometry and the processing of NF-κB2 p100 into p52 was determined as [(signal of p52)/(signal of p100+ signal of p52)] x 100. The plot depicts the mean and SEM of fold change in p52 levels after the addition of BAFF. Data are pooled from 3 independent

experiments (2 technical replicates/experiment). ns, not significant (Kruskal-Wallis test with Dunn's correction).

**E. Similar TRAF3 recruitment to BAFFR in B cell lines expressing different isotypes.** DG-75 cells expressing IgM, IgD, IgA1, or IgG1 isotypes were incubated for 0 - 30 min with FLAG-tagged BAFF followed by co-immunoprecipitation with anti-FLAG M2 mAb-coupled agarose beads and western blot analysis for TRAF3 and BAFFR. Immunoprecipitates of untreated cells (-) were used as control for unspecific binding. N-fold changes of TRAF3 were calculated as signals normalized to BAFFR and further normalized to the sample treated with BAFF for 5 min on ice (t=0) per each cell line.

**F. Kinetics of AKT phosphorylation (S473) in B cell lines expressing different isotypes in response to BCR activation.** Cells were incubated with F(ab')<sub>2</sub> anti-IgM (2 µg/mL), F(ab')<sub>2</sub> anti-IgD (2 µg/mL), or recombinant SARS-CoV-2 spike protein (1µg/mL) for 2 - 60 min and analyzed by western blot for pAKT (S473); β-actin was used as a loading control. The western blots are representative of ≥2 independent experiments. N-fold changes were calculated relative to the t=0 sample of each cell line.

**G. Similar kinetics of AKT phosphorylation (S473) in B cell lines expressing anti-spike IgM and native IgM and IgD BCRs.** DG-75 cells expressing native IgM or IgD, anti-spike IgM or dual positive cells (native IgD/anti-spike IgM) were treated with BAFF (100 ng/mL) for 2 - 60 min and analyzed by western blot for pAKT (S473). After densitometric analysis of signal intensities, the changes in pAKT signals were calculated as [(signal t<sub>x</sub>-signal t<sub>0</sub>)/signal t<sub>0</sub>]. Plot shows the mean and SEM of ≥5 independent experiments. \*\*p<0.01 (Mann-Whitney test)

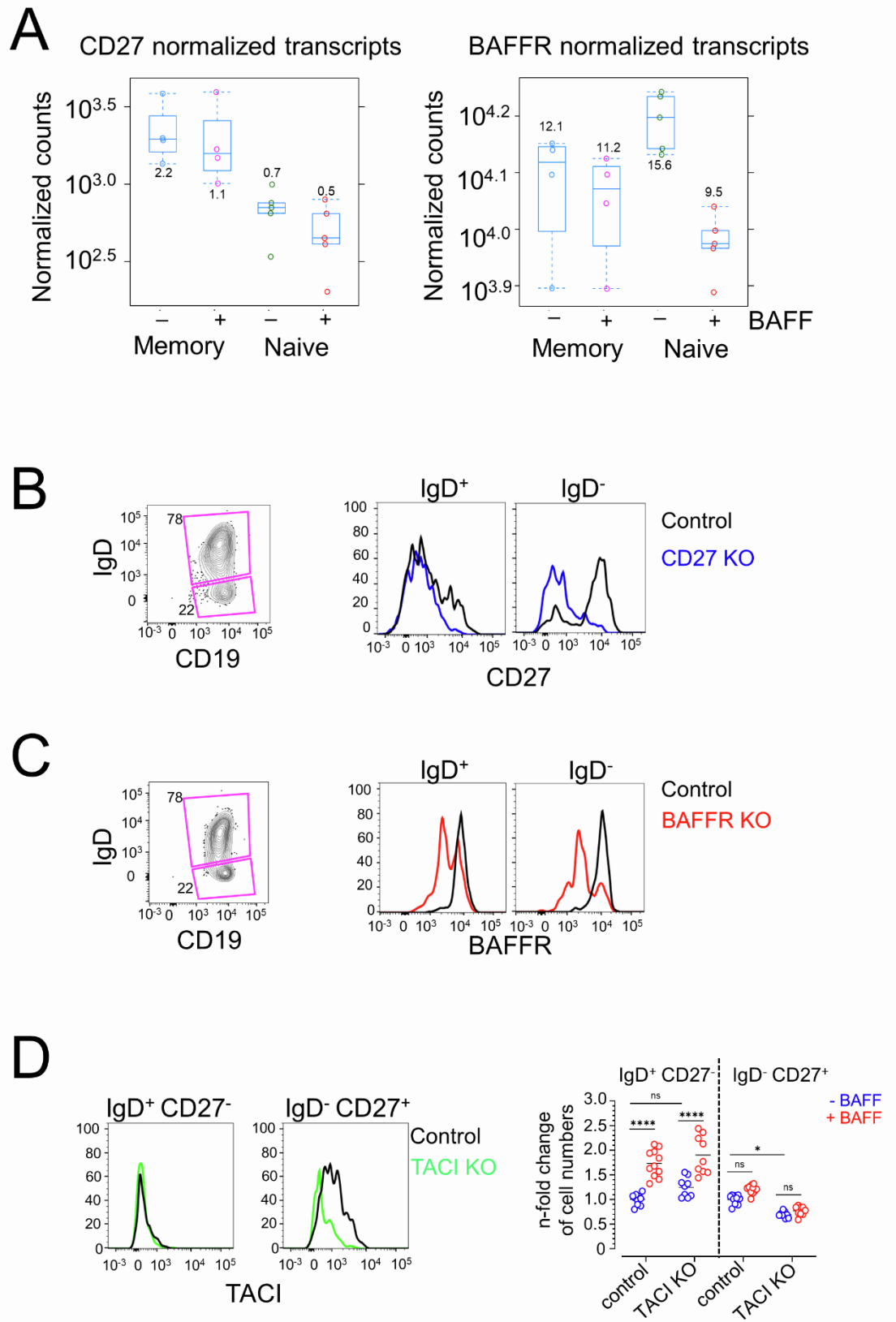


**Figure S6 (related to Figure 7). Inactivation of *CD27* and *BAFFR* in primary B cells.**

**A. Levels of *CD27* and *BAFFR* transcripts expressed by naive and switched memory B cells.** Naive and memory B cells were cultivated with BAFF (20 ng/mL) or left untreated for 6 h as described in Figure 2. The box plots represent the normalized gene expression showing the spread as boxes, means (numerical values) as lines, the individual values as dots. RNA-Seq was performed as described in Figure 2.

**B. Inactivation of *CD27* by CRISPR-Cas9.** B cells were electroporated with a *CD27*-gRNA/Cas9 RNP complex or without an RNP complex (control). Cells were cultivated for 5 days and analyzed by flow cytometry for the expression of *CD27*. *CD19*<sup>+</sup> B cells were gated according to the expression of *IgD* into *IgD*<sup>+</sup> (naive and MZ) and *IgD*<sup>-</sup> memory B cells.

**C. Inactivation of *TNFRSF13C* in human B cells.** Cells were electroporated with a gRNA-Cas9 RNP complex targeting the exon 2 of the *TNFRSF13C* gene. Cells electroporated under the same conditions without a gRNA-Cas9 RNP complex served as controls. Electroporation of B cells with the *BAFFR*-gRNA/Cas9 RNP complex resulted in > 50% reduction of *BAFFR* expression in naive and MZ (*IgD*<sup>+</sup>) B cells and in >70% in memory (*IgD*<sup>-</sup>) B cells after 5 days of cultivation.

**D. Loss of *TACI* does not restore responsiveness of memory B cells to *BAFF*.** B cells were electroporated with a *TACI*-gRNA/Cas9 RNP complex or without an RNP complex (control) and analyzed by flow cytometry and timed acquisition. (left) Histogram overlays show *TACI* expression in *IgD*<sup>+</sup> *CD27*<sup>-</sup> (naive) and *IgD*<sup>-</sup> *CD27*<sup>+</sup> (memory) B cells at day 5. (right) Loss of *TACI* does not affect *BAFF*-induced survival of B cell subsets. At day 2 after electroporation, cells were treated with *BAFF* (20 ng/ml) or left untreated for additional 3 days. Cell numbers

were evaluated by flow cytometry and timed acquisition. N-fold change in cell numbers was calculated as [cell numbers  $\pm$ gTACI-RNP  $\pm$ BAFF/cell numbers wo RNP wo BAFF] per each subset. Plot shows the mean of two independent experiments with two healthy donors ( $\geq 4$  replicates per condition). \*\*\*\* $p < 0.0001$ ; \* $p < 0.05$ ; ns, not significant (2-way ANOVA with Tukey multiple comparisons test).